

# PROJECTIVE LINKS

**THE SIGNATURE AND DETERMINANT  
OF A LINK IN  $\mathbb{RP}^3$**

**Jeffrey Marshall-Milne, BA**

A Thesis Submitted to the School of Graduate Studies in Partial  
Fulfillment of the Requirements for the Degree Master of Science

Department of Mathematics and Statistics  
McMaster University

McMaster University © Copyright by Jeffrey Marshall-Milne, April 2025

DEGREE: MASTER OF SCIENCE, 2025

UNIVERSITY: McMaster University, Hamilton, Ontario

DEPARTMENT: Mathematics and Statistics

TITLE: The Signature and Determinant of a Link in  $\mathbb{R}P^3$

AUTHOR: Jeffrey Marshall-Milne, BA (York University)

SUPERVISORS: Professor Hans U. Boden and Professor Ian Hambleton

NUMBER OF PAGES: x, 37

# Lay Abstract

A knot is a closed loop of string. This paper studies knots in a 3-dimensional space called real projective space. We find that knots in real projective space often behave very similarly to knots in Euclidean space (the space you and I inhabit), and we unveil certain interesting phenomena unique to real projective space.

# Abstract

The Gordon-Litherland pairing  $\mathcal{G}_F$  of a surface  $F$  generalizes the symmetrized Seifert pairing by allowing  $F$  to be nonorientable. The pairing  $\mathcal{G}_F$  is developed for surfaces in real projective 3-space  $\mathbb{R}P^3$ , leading to signature and determinant invariants of links  $L \subseteq \mathbb{R}P^3$ . The set of spanning surfaces of  $L$  (i.e. surfaces in  $\mathbb{R}P^3$  bounding  $L$ ) is partitioned into two classes by an equivalence relation called  $S^*$ -equivalence. It is shown that only one of these classes contains orientable surfaces. Consequently, two distinct signature and determinant invariants arise. This contrasts the case of links in  $S^3$ , where the pairing  $\mathcal{G}_F$  determines a unique signature and determinant, and the case of links in thickened surfaces, where signatures and determinants come in unordered pairs. Explicit computational methods are given.

To Matthew, my best friend.

# Acknowledgments

I would like to thank my supervisor Hans U. Boden, whose research my thesis extends, and whose guidance has shaped me into the knot theorist I am today. I would also like to thank my supervisor Ian Hambleton for teaching me all the algebra I know – it has been an immense privilege having your encyclopedic knowledge at my disposal. I must also extend my gratitude to committee member Patrick Naylor for always finding the time to give me thoughtful feedback, and to all the members of McMaster’s knot theory group, such as Mahan Moazzeni and Geunyoung Kim, for enduring my mathematical ramblings for the past year. In particular, I owe a special thanks to Hodayun Karimi, for setting the stage for my thesis with his previous research, and for always making time to help me understand research papers. Finally, I thank my parents Kate Marshall and Rod Milne, to whom I owe everything.

# Contents

<b>1</b>	<b>Introduction</b>	<b>1</b>
<b>2</b>	<b>Spanning Surfaces</b>	<b>3</b>
2.1	Link Diagrams . . . . .	3
2.2	Nullhomologous Links . . . . .	5
2.3	$S^*$ -Equivalence of Spanning Surfaces . . . . .	7
2.4	$S$ -Equivalence of Seifert Surfaces . . . . .	10
<b>3</b>	<b>The Parity of a Surface in <math>\mathbb{RP}^3</math></b>	<b>14</b>
3.1	Linking Number . . . . .	14
3.2	The Parity of a Surface in $\mathbb{RP}^3$ . . . . .	16
3.2.1	Euler number . . . . .	16
3.2.2	Betti number . . . . .	17
3.2.3	Parity . . . . .	19
<b>4</b>	<b>The Gordon-Litherland Pairing</b>	<b>22</b>
4.1	The Gordon-Litherland Pairing . . . . .	22
4.2	Elementary Properties . . . . .	24
4.2.1	Reflection . . . . .	24
4.2.2	Split links . . . . .	25
4.2.3	Connected sums . . . . .	25
4.2.4	Affine links . . . . .	26
4.3	Computing the Gordon-Litherland Pairing . . . . .	27
4.3.1	Consequences for knots . . . . .	29
4.3.2	Consequences for links of two homologically nontrivial components . . . . .	31
4.3.3	Unoriented links . . . . .	32
4.4	Alternating Links . . . . .	32
<b>5</b>	<b>Discussion</b>	<b>35</b>

# List of Figures

2.1	Disk diagrams. . . . .	4
2.2	Reidemeister moves. . . . .	4
2.3	Generalized Reidemeister moves. . . . .	5
2.4	The left and middle diagrams depict checkerboard colourings. The right diagram is <i>not</i> a checkerboard colouring. . . . .	5
2.5	The moves generating $S^*$ -equivalence. . . . .	7
2.6	Local configurations. . . . .	8
2.7	The checkerboard colouring of $D$ determines a checkerboard colouring of $D'$ in a natural way. . . . .	9
2.8	An oriented smoothing. . . . .	10
2.9	The Seifert algorithm applied to a classical link diagram. . . . .	11
2.10	The Seifert algorithm applied to a diagram of a nullhomologous link. . . . .	12
2.11	An ambient isotopy before attaching a thin tube. . . . .	13
3.1	A diagram of the preimage in $S^3$ of a link in $\mathbb{RP}^3$ . . . . .	15
3.2	Type and index of a crossing. . . . .	16
3.3	Local contributions to $\frac{1}{2}e(F, L)$ at a crossing ( $F$ is the shaded surface). . . . .	17
3.4	Homology of checkerboard surfaces. . . . .	18
3.5	Crossing types. . . . .	18
3.6	Resolving a ribbon intersection. . . . .	20
4.1	Connect sum link. . . . .	26
4.2	Dual checkerboard surfaces and their bases. . . . .	28
4.3	Diagram of $U_2$ . . . . .	31
4.4	On the left, $a$ is in red and $b$ is in blue. The curve on the right has the same image in $H_1(B; \mathbb{Z})$ as the curve on the left. . . . .	34

# List of Abbreviations and Symbols

$\mathbb{C}$	Complex numbers
$\mathfrak{g}_F(L)$	Gordon-Litherland numbers of $F$ determined by $L$
$\mathbb{R}P^3$	Real projective 3-space
$\sigma_F(L)$	$F$ -signature of $L$
$\det_F(L)$	$F$ -determinant of $L$
$\text{null}_F(L)$	$F$ -nullity of $L$
$\text{Parity}(F, L)$	Parity of $F$
$\tilde{D}$	Disk diagram
$\mathbb{Z}$	Integers
$\mathbb{Z}/2$	Cyclic group of order 2
$b_1(F)$	First Betti number of the surface $F$
$D$	Diagram
$e(F, L)$	Euler number of the surface $F$
$F$	Surface
$H_1(X; \mathbb{Z})$	Singular homology group of $X$ with coefficients in $\mathbb{Z}$
$H_1(X; \mathbb{Z}/2)$	Singular homology group of $X$ with coefficients in $\mathbb{Z}/2$
$K$	Knot
$L$	Link
$S^3$	3-sphere

# Declaration of Academic Achievement

I, Jeffrey Marshall-Milne, declare that this research paper is entirely my own work, save when explicitly stated otherwise. All necessary citations have been included, and I understand the consequences of academic dishonesty.

# Chapter 1

## Introduction

In 1978, Gordon and Litherland introduced a symmetric bilinear map  $\mathcal{G}_F$  (now called the *Gordon-Litherland pairing*) which generalizes the symmetrized Seifert pairing, thereby allowing for the computation of a link's signature from a possibly nonorientable surface [15]. The pairing  $\mathcal{G}_F$  has garnered a lot of attention in recent years due to the work of Greene and Howie who (independently) used it to give a topological characterization of alternating links in  $S^3$  [9][10]. Even more recently, Boden and Karimi extended this characterization to links in thickened surfaces [4].

The object of this paper is to develop the Gordon-Litherland pairing in real projective 3-space  $\mathbb{R}P^3$ , highlighting certain interesting phenomena unique to the projective setting. In particular, the pairing is seen to give rise to two distinct sets of invariants (which contrasts the classical and thickened surface settings).

An equivalence relation on spanning surfaces of a link  $L \subseteq \mathbb{R}P^3$  (called  $S^*$ -equivalence) is generated by ambient isotopies, attaching thin tubes, and attaching small half-twisted bands. In §2.3, checkerboard surfaces are used to show that to each link  $L$  is associated exactly two  $S^*$ -equivalence classes. In §2.4, algorithm surfaces (a kind of orientable spanning surface) are used to show that there is a preferred  $S^*$ -equivalence class. §3.2 develops an easily computed invariant, the parity of a surface, which picks out the preferred  $S^*$ -equivalence class. The Gordon-Litherland pairing is developed in §4 and, as a consequence of the preferred  $S^*$ -equivalence class, two distinct sets of link invariants arise. We discuss the elementary behaviour of these invariants, and we generalize a handful of classical results. Finally, we discuss alternating links in §4.4, where we establish one direction of a Greene-Howie-type characterization of alternating links in  $\mathbb{R}P^3$  (the easy direction). This is applied to generalize Murasugi's classical result on the chirality of special alternating links [19].

Links in  $\mathbb{RP}^3$  were originally considered by Oleg Viro in 1985 [22], with Julia Viro (who went by Julia Drobotukhina at the time) following up in 1990 with a generalization of the Jones polynomial, using it to prove the Tate conjecture in  $\mathbb{RP}^3$  [5]. We highlight some of the important work done in projective link theory since then. The classifications of rational projective links and of projective links of at most six crossings were settled by Julia Viro in 1991 [7][6]. In 2003, Mroczkowski studied the diagrammatic unknotting of links in  $\mathbb{RP}^3$  [17] and applied these results to develop the HOMFLYPT and Kauffman bracket skein modules in  $\mathbb{RP}^3$  [18]. The study of polynomial invariants in  $\mathbb{RP}^3$  was carried further by Huynh and Le in 2008, who studied the twisted Alexander polynomial [11]. The next natural step is to categorify these polynomials. Indeed, the 2004-2013 work of Asaeda-Przytycki-Sikora, Manturov, and Gabrovsek developed a Khovanov-type homology for links in  $\mathbb{RP}^3$  [1][14][8]. The study of links in  $\mathbb{RP}^3$  has been particularly popular in recent years, as illustrated by Viro and Viro's 2021 paper relating properties of a link to properties of its exterior's fundamental group [21], by Mishra and Narayanan's 2023 work establishing certain criteria for a link in  $\mathbb{RP}^3$  to be affine [16], by Manolescu and Willis's 2023 work on the  $s$ -invariant in  $\mathbb{RP}^3$  [13], by Kauffman, Mishra, and Narayanan's 2024 work on the Kauffman bracket polynomial in  $\mathbb{RP}^3$  [12], and by the 2024 work of Purcell and Su on the hyperbolic structure of alternating link complements in oriented thickenings of nonorientable surfaces [20].

# Chapter 2

## Spanning Surfaces

In §2.1 we describe diagrams of links in  $\mathbb{RP}^3$ , and in §2.2 we discuss the many equivalent definitions of a nullhomologous link. In §2.3 we partition the set of (possibly nonorientable) spanning surfaces of  $L$  into two distinct classes, and in §2.4 we show that only one of these classes contains all Seifert surfaces.

### 2.1 Link Diagrams

A closed 1-dimensional manifold  $L$  smoothly embedded in a 3-manifold  $M$  is called a *link* (or a *knot*, if  $L$  is connected). The present paper is primarily concerned with oriented links up to the equivalence relation of ambient isotopy. The mapping class group of  $\mathbb{RP}^3$  is isomorphic to  $\mathbb{Z}/2$  (generated by reflection about a projective plane), so for oriented links in  $\mathbb{RP}^3$ , the equivalence relations of ambient isotopy and ambient orientation-preserving homeomorphism are identical.

Let  $P \in \mathbb{RP}^3$  denote the image of the north and south poles  $N, S \in S^3$ . Note that the projection map  $S^3 \setminus \{N, S\} = S^2 \times \mathbb{R} \rightarrow S^2$  commutes with the antipodal map, thereby inducing a map  $p : \mathbb{RP}^3 \setminus \{P\} = \mathbb{RP}^2 \tilde{\times} \mathbb{R} \rightarrow \mathbb{RP}^2$  and allowing for the diagrammatic study of links in  $\mathbb{RP}^3$ .

In greater detail: let  $L \subseteq \mathbb{RP}^3$  be a link. If necessary, perturb  $L$  via a small ambient isotopy to ensure that  $L \cap P = \emptyset$  and  $L$  is in general position with respect to  $p$ . In other words, the image  $D = p(L) \subseteq \mathbb{RP}^2$  is a 4-valent topological graph. The projective plane is nonorientable, so we ought to be careful with our description of over/under information at the vertices (or *crossings*) of  $D$ . In a small disk neighborhood of a crossing  $c$ , the diagram  $D$  is shaped like an X (i.e. the union of two open intervals  $A$  and  $B$  intersecting once in a transverse double point). The over/under information is specified

by a bijection  $\{\text{local orientations at } c\} \rightarrow \{A \text{ over } B, B \text{ over } A\}$  (a local orientation at  $c$  may be thought of as an isomorphism  $H_2(\mathbb{RP}^2, \mathbb{RP}^2 \setminus \{c\}; \mathbb{Z}) \rightarrow \mathbb{Z}$ ).

In this way, we may conceive of links in  $\mathbb{RP}^3$  as compact 4-valent topological graphs embedded in  $\mathbb{RP}^2$  with over/under information specified at each vertex. The graph  $D$  is called a *diagram* of  $L$ . If  $\mathbb{RP}^1$  is a homologically nontrivial simple closed curve in  $\mathbb{RP}^2$  intersecting  $D$  in general position, then by cutting along  $\mathbb{RP}^1$  we obtain a *disk diagram* of  $L$  (i.e. a depiction of  $L$  as a topological graph  $\tilde{D} \subseteq \mathbb{D}^2$ ). While disk diagrams provide a useful means of visualization (see Figure 2.1), whenever possible, we opt to work instead with diagrams in  $\mathbb{RP}^2$  as they are more intrinsic to  $\mathbb{RP}^3$ .

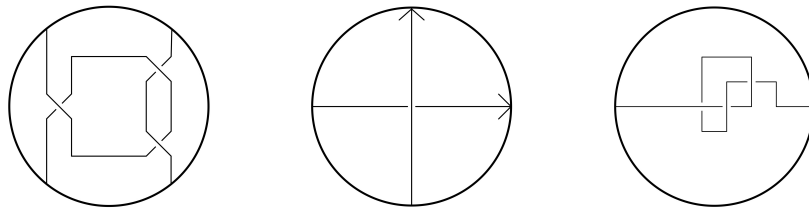


Figure 2.1: Disk diagrams.

As in the classical and thickened surface settings, links  $L, L' \subseteq \mathbb{RP}^3$  with diagrams  $D, D' \subseteq \mathbb{RP}^2$  will be ambient isotopic if and only if  $D$  is related to  $D'$  via the three Reidemeister moves (see R1, R2, and R3 of Figure 2.2).

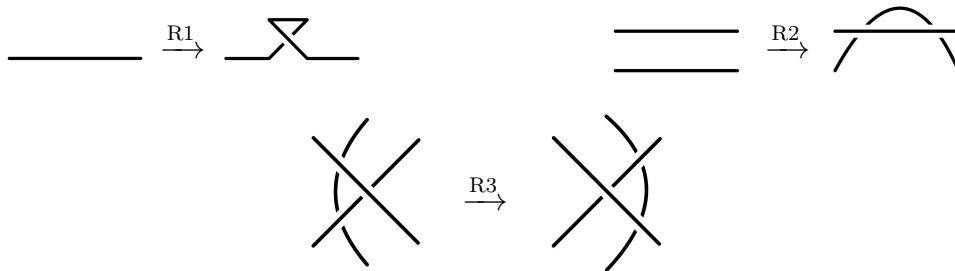


Figure 2.2: Reidemeister moves.

On the level of disk diagrams  $\tilde{D} \subseteq \mathbb{D}^2$ , we need to introduce two *generalized Reidemeister moves* to move across the boundary  $\partial\mathbb{D}^2$  (see R4 and R5 of Figure 2.3).

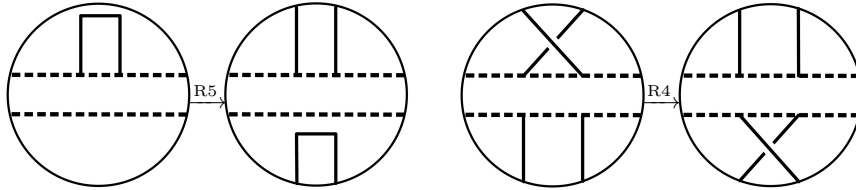


Figure 2.3: Generalized Reidemeister moves.

## 2.2 Nullhomologous Links

For a link  $L$  in a 3-manifold  $M$ , a *spanning surface* of  $L$  is a compact surface  $F$  smoothly embedded in  $M$  and bounding  $L$  (note that  $F$  is not necessarily orientable or connected). If  $L$  is oriented, then an oriented spanning surface  $F$  whose orientation induces the orientation of  $L$  is called a *Seifert surface*. An oriented link  $L \subseteq M$  is called *nullhomologous* if  $[L] = 0 \in H_1(M; \mathbb{Z})$ .

A diagram  $D \subseteq \mathbb{RP}^2$  of  $L$  is said to be *checkerboard colourable* if there exists a map  $f : \{\text{components of } \mathbb{RP}^2 \setminus D\} \rightarrow \{\text{black, white}\}$  such that components whose closures in  $\mathbb{RP}^2$  intersect in a 1-dimensional cell complex are mapped to different colours (see Figure 2.4). If  $D$  is checkerboard coloured, then the black faces determine a spanning surface  $B$ , and the white faces determine a spanning surface  $W$ . The surfaces  $B$  and  $W$  are called *checkerboard surfaces* and are said to be *dual* to one another. Note, in particular, that links admitting a checkerboard colourable diagram are nullhomologous.

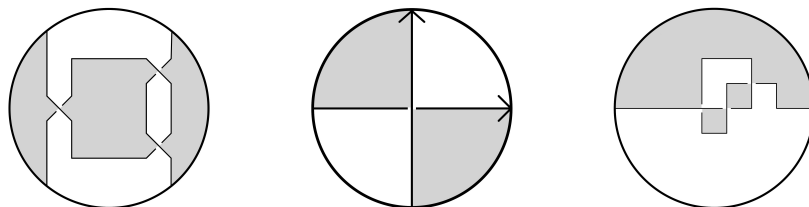


Figure 2.4: The left and middle diagrams depict checkerboard colourings. The right diagram is *not* a checkerboard colouring.

**Proposition 2.1** (characterization of nullhomologous links). *Let  $L \subseteq \mathbb{RP}^3$  be an oriented link. The following are equivalent.*

- (1)  $[L] = 0 \in H_1(\mathbb{RP}^3; \mathbb{Z})$ .
- (2)  $L$  admits a Seifert surface.
- (3)  $L$  admits a spanning surface.
- (4) The mod 2 intersection number of  $L$  with an embedded projective plane  $\mathbb{RP}^2 \subseteq \mathbb{RP}^3$  equals zero.
- (5)  $L$  is checkerboard colourable.

Note that on the level of a disk diagram  $\tilde{D} \subseteq \mathbb{D}^2$ , the equivalence (1)  $\Leftrightarrow$  (4) says that  $\tilde{D}$  represents a nullhomologous link if and only if  $|\tilde{D} \cap \partial\mathbb{D}^2|$  is a multiple of 4 (for example, the diagrams on the left and in the middle of Figure 2.1 depict nullhomologous links, while the diagram on the right depicts a homologically nontrivial link).

*Proof of Proposition 2.1.* The implication (1)  $\Rightarrow$  (2) is a basic exercise in algebraic topology, and the implication (2)  $\Rightarrow$  (3) is definitional. Next we argue that (1)  $\Leftrightarrow$  (4).

Note that  $H_2(\mathbb{RP}^3; \mathbb{Z}/2) \cong \text{Hom}(H_1(\mathbb{RP}^3; \mathbb{Z}), \mathbb{Z}/2)$  by duality and the universal coefficient theorem, with  $H_2(\mathbb{RP}^3; \mathbb{Z}/2) \cong \mathbb{Z}/2$  generated by  $\mathbb{RP}^2$ , and  $\text{Hom}(H_1(\mathbb{RP}^3; \mathbb{Z}), \mathbb{Z}/2)$  generated by intersection with  $\mathbb{RP}^2$ . So, a link  $L \subseteq \mathbb{RP}^3$  is nullhomologous if and only if  $L$  has even intersection number with a projective plane, as desired.

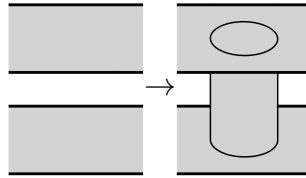
If  $L$  is checkerboard colourable, then  $L$  has a spanning surface (just take a checkerboard surface), so  $[L] = 0 \in H_1(\mathbb{RP}^3; \mathbb{Z}/2)$ . In the special case of  $\mathbb{RP}^3$ , this is clearly equivalent to  $[L] = 0 \in H_1(\mathbb{RP}^3; \mathbb{Z})$ . This proves (5)  $\Rightarrow$  (1). The proof will be complete when we establish the implication (1)  $\Rightarrow$  (5).

If  $L \subseteq \mathbb{RP}^3$  is nullhomologous and  $D \subseteq \mathbb{RP}^2$  is a diagram of  $L$ , then a checkerboard colouring is obtained as follows. Fix a component  $Y$  of  $\mathbb{RP}^2 \setminus D$  and colour  $Y$  black. For another component  $Y'$ , fix points  $y \in Y$  and  $y' \in Y'$ , as well as a path  $\alpha \subseteq \mathbb{RP}^2$  from  $y$  to  $y'$  intersecting  $D$  in general position. If  $\alpha$  intersects  $D$  in an even number of points, colour  $Y'$  black. Otherwise, colour  $Y'$  white. To see that this does not depend on our choice of  $\alpha$ , note that  $H_1(\mathbb{RP}^2; \mathbb{Z}/2) \cong \text{Hom}(H_1(\mathbb{RP}^2; \mathbb{Z}), \mathbb{Z}/2)$  by duality and the universal coefficient theorem. Since  $L$  is nullhomologous, it follows that  $D$  has even intersection number with every element of  $H_1(\mathbb{RP}^2; \mathbb{Z})$ . Two paths  $\alpha$  and  $\alpha'$  from  $y$  to  $y'$  together determine an element of  $H_1(\mathbb{RP}^2; \mathbb{Z})$ , so the parities of their intersection numbers with  $D$  must coincide.  $\square$

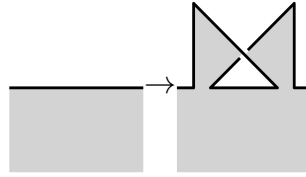
Moreover, we showed that if  $L \subseteq \mathbb{RP}^3$  is nullhomologous, then every diagram of  $L$  is checkerboard colourable.

## 2.3 $S^*$ -Equivalence of Spanning Surfaces

Let  $L \subseteq \mathbb{RP}^3$  be a nullhomologous link. We define  $S^*$ -equivalence to be the equivalence relation on spanning surfaces of  $L$  generated by ambient isotopies and the moves pictured in Figure 2.5.



Move 1: Attaching a thin tube.



Move 2: Attaching a small half-twisted band.

Figure 2.5: The moves generating  $S^*$ -equivalence.

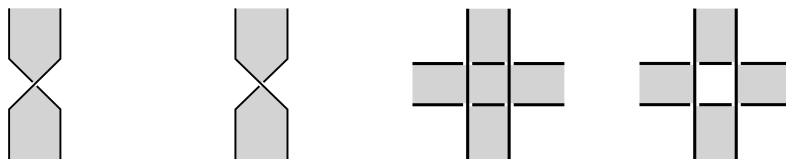
By a *thin tube*, we mean a 1-handle which admits a filling in  $\mathbb{RP}^3$ . Although Figure 2.5 only displays a small half-twisted band with a right-handed half-twist, left-handed half-twists are also permitted.

**Theorem 2.2.** *A nullhomologous link  $L \subseteq \mathbb{RP}^3$  admits exactly two  $S^*$ -equivalence classes of spanning surfaces. If  $B$  and  $W$  are the checkerboard surfaces of some diagram of  $L$ , then  $B$  and  $W$  represent the two  $S^*$ -equivalence classes.*

Our three-part proof of Theorem 2.2 mirrors [3], where the analogous result is established for links in thickened surfaces. *Part 1: every spanning surface of  $L$  is  $S^*$ -equivalent to a checkerboard surface.* We state this as a lemma so that it may be used later.

**Lemma 2.3.** *Let  $L \subseteq \mathbb{RP}^3$  be a nullhomologous link with spanning surface  $F$ . Then  $F$  is  $S^*$ -equivalent through ambient isotopies and attaching thin tubes to a checkerboard surface.*

*Proof.* By attaching thin tubes, we may assume  $F$  does not have closed components. So, there is a topological graph  $G$  contained in a small closed neighborhood  $F' \subseteq F$  such that  $F$  is ambient isotopic to  $F'$ . If necessary, perturb  $F'$  via a small ambient isotopy to ensure that  $F' \cap P = \emptyset$  (here  $P$  denotes the image of the north and south poles  $N, S \in S^3$  under the map  $S^3 \rightarrow \mathbb{RP}^3$ ). Take  $F'$  to be in general position with the respect to the projection map  $p : \mathbb{RP}^3 \setminus \{P\} \rightarrow \mathbb{RP}^2$ . In other words, the self-intersections of  $p(F)$  occur in finitely many of the local configurations 1-3 pictured in Figure 2.6. Turn each instance of Configuration 3 into an instance of Configuration 4 by attaching a thin tube. Note that the resulting surface is a checkerboard surface.  $\square$



Configuration 1. Configuration 2. Configuration 3. Configuration 4.

Figure 2.6: Local configurations.

*Part 2:* If  $B$  and  $W$  are the checkerboard surfaces of a diagram  $D \subseteq \mathbb{RP}^2$  of  $L$ , then every checkerboard surface of  $L$  is  $S^*$ -equivalent to  $B$  or to  $W$ . Indeed, if  $D'$  is another diagram of  $L$ , then  $D$  is related to  $D'$  by a sequence of Reidemeister moves (see Figure 2.2). The checkerboard colouring of  $D$  determines a checkerboard colouring of  $D'$  in a natural way (see Figure 2.7). Move 2 of Figure 2.5 illustrates the situation where  $D'$  is obtained from  $D$  by a Reidemeister 1 move. We see clearly that for the checkerboard surfaces  $B'$  and  $W'$  of  $D'$ , we have  $B'$  obtained from  $B$  by attaching a small half-twisted band, and  $W'$  obtained from  $W$  by an ambient isotopy. As shown in [23], the Reidemeister 2 and 3 moves also correspond to  $S^*$ -equivalences

on the level of checkerboard surfaces. This proves Part 2

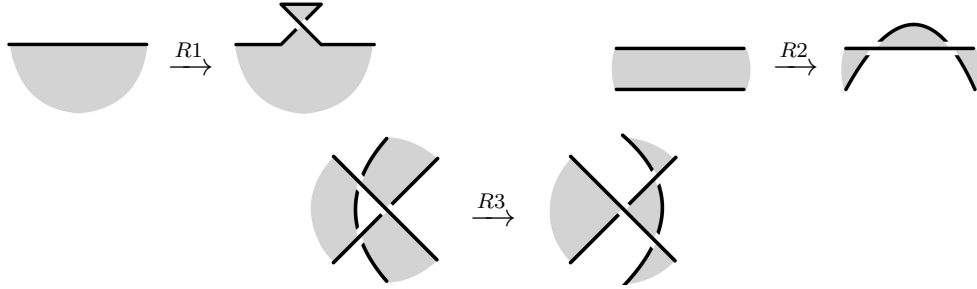


Figure 2.7: The checkerboard colouring of  $D$  determines a checkerboard colouring of  $D'$  in a natural way.

*Part 3: If  $B$  and  $W$  are the checkerboard surfaces of a diagram  $D \subseteq \mathbb{RP}^2$ , then  $B$  is not  $S^*$ -equivalent to  $W$ . This is an easy consequence of the following theorem.*

**Theorem 2.4.** *Let  $F$  and  $F'$  be spanning surfaces of link  $L \subseteq \mathbb{RP}^3$ . The surfaces  $F$  and  $F'$  are  $S^*$ -equivalent if and only if  $[F] = [F'] \in H_2(\mathbb{RP}^3, L; \mathbb{Z}/2)$ .*

*Proof.* ( $\Rightarrow$ ) The argument is identical to the proof of [3, Lemma 1.5] and amounts to verifying the invariance of  $[F]$  under the moves generating  $S^*$ -equivalence. For example, certainly  $[F]$  is invariant under ambient isotopies. Invariance under attaching a thin tube is seen just as easily: if  $F'$  is obtained from  $F$  by attaching a thin tube, then the difference  $[F'] - [F]$  is a 2-sphere bounding a 3-ball.

( $\Leftarrow$ ) Assume  $[F] = [F']$ . Note that  $H_2(L; \mathbb{Z}/2) = 0$ , so an injection  $H_2(\mathbb{RP}^3; \mathbb{Z}/2) \rightarrow H_2(\mathbb{RP}^3, L; \mathbb{Z}/2)$  falls out of the long exact sequence of the pair  $(\mathbb{RP}^3, L)$  (see (1) below). It follows that  $[\mathbb{RP}^2] \neq 0 \in H_2(\mathbb{RP}^3, L; \mathbb{Z}/2)$ .

$$\cdots \rightarrow H_2(L; \mathbb{Z}/2) \rightarrow H_2(\mathbb{RP}^3; \mathbb{Z}/2) \rightarrow H_2(\mathbb{RP}^3, L; \mathbb{Z}/2) \rightarrow \cdots \quad (1)$$

Let  $B$  and  $W$  be the checkerboard surfaces of some diagram of  $L$ . By Parts 1 and 2 above,  $F$  is  $S^*$ -equivalent to  $B$  or to  $W$ , and similarly for  $F'$ . Without loss of generality, assume  $F$  is  $S^*$ -equivalent to  $B$ . Assume for contradiction  $F'$  is  $S^*$ -equivalent to  $W$ . Then  $[F] + [F'] = [B] + [W] = [\mathbb{RP}^2] \neq 0$  by the first part of the proof (i.e. the  $\Rightarrow$  direction treated in the previous paragraph), contradicting the fact that  $[F] = [F']$ . We conclude that  $F'$  is  $S^*$ -equivalent to  $B$ , and therefore also to  $F$ , thereby completing the proof.  $\square$

To prove Part 3, note that  $[B] + [W] = [\mathbb{RP}^2] \neq 0 \in H_2(\mathbb{RP}^3, L; \mathbb{Z}/2)$ , so  $B$  is not  $S^*$ -equivalent to  $W$  by Theorem 2.4.

Parts 1, 2, and 3 combine to prove Theorem 2.2.

## 2.4 $S$ -Equivalence of Seifert Surfaces

$S$ -equivalence is the equivalence relation on Seifert surfaces of  $F$  generated by ambient isotopies and attaching thin tubes (see Move 1 of Figure 2.5). Note that tube attachment is now required to preserve orientability. The purpose of this subsection is to prove the following.

**Theorem 2.5.** *If  $L \subseteq \mathbb{RP}^3$  is a nullhomologous oriented link with Seifert surfaces  $F$  and  $F'$ , then  $F$  is  $S$ -equivalent to  $F'$ .*

We stress the importance that Seifert surfaces are not only orientable, but come endowed with an orientation inducing the orientation of  $L$ . For example, the oriented link in the middle of Figure 2.4 has both checkerboard surfaces  $B$  and  $W$  being orientable, but only  $B$  can be oriented compatibly with  $L$ .

The proof of Theorem 2.5 is in two parts and is entirely analogous to the proof of Theorem 2.2 (we mirror the methods of [2] used for links in  $S^3$ ). Just as we needed checkerboard surfaces to prove Theorem 2.2, we will need *algorithm surfaces* (definition to come) to prove Theorem 2.5. Let us start by recalling the *Seifert algorithm* for links in  $S^3$ , which inputs a diagram  $D \subseteq \mathbb{R}^2$  of an oriented link  $L \subseteq S^3$ , and outputs a Seifert surface  $F(D) \subseteq S^3$  in a canonical way (see Figure 2.9).

**Algorithm 2.6** (Seifert Algorithm in  $S^3$ ). *Step 1.* Perform an *oriented smoothing* (see Figure 2.8) at each crossing of  $D$  to obtain a collection of mutually disjoint oriented simple closed curves  $C_i \subseteq \mathbb{R}^2$  (called *Seifert circles*).

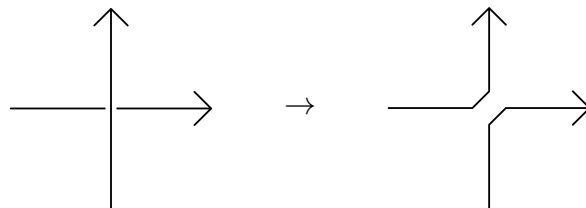


Figure 2.8: An oriented smoothing.

*Step 2.* Each  $C_i$  bounds a unique closed disk  $B_i \subseteq \mathbb{R}^2$  (called a *Seifert disk*). Orient  $B_i$  by labeling one side as “up” and the other side as “down,” with the convention that the orientation of  $C_i$  runs counterclockwise when the up side is viewed from above.

*Step 3.* Let  $d(C_i)$  denote the *depth* of  $C_i$  (i.e. the number of Seifert disks  $B_j$  containing  $C_i$  in their interior). Translate  $B_i$  by  $d(C_i)$  units in the upwards direction (towards the reader).

*Step 4.* Attach half-twisted bands to the disks  $B_i$  in accordance with the crossings of  $D$  to recover a Seifert surface  $F(D)$  of  $L$ .

**Definition 2.7.** A Seifert surface of  $L$  obtained via the Seifert algorithm is called an *algorithm surface*.



Figure 2.9: The Seifert algorithm applied to a classical link diagram.

There are two issues one encounters in generalizing the algorithm to nullhomologous oriented links in  $\mathbb{R}P^3$ . *Issue 1.* A priori, there is no guarantee that each of the Seifert circles  $C_i \subseteq \mathbb{R}P^2$  will bound unique disks  $B_i \subseteq \mathbb{R}P^2$ , thus complicating Step 2. *Issue 2.*  $\mathbb{R}P^2$  is nonorientable, so there is no globally defined “upwards direction,” thereby complicating Step 3.

To resolve Issue 1, assume for contradiction we have a nullhomologous oriented link  $L \subseteq \mathbb{R}P^3$  with diagram  $D \subseteq \mathbb{R}P^2$ , and one of the Seifert circles  $C_i \subseteq \mathbb{R}P^2$  obtained after an oriented smoothing at each crossings does not bound a disk in  $\mathbb{R}P^2$ . It is not hard to see that up to ambient isotopy, there are two types of simple closed curves in  $\mathbb{R}P^2$ : those which bound a unique disk in  $\mathbb{R}P^2$ , and those which are nontrivial in  $H_1(\mathbb{R}P^2; \mathbb{Z}) \cong \mathbb{Z}/2$  (to see this, just look at preimages in  $S^2$ ). Since  $[C_i] \neq 0 \in H_1(\mathbb{R}P^2; \mathbb{Z})$ , it follows that the complement of  $C_i$  in  $\mathbb{R}P^2$  is homeomorphic to the complement of  $\mathbb{R}P^1$  (i.e. homeomorphic to an open disk). Moreover  $C_j \subseteq \mathbb{R}P^2 \setminus C_i$  for all  $j \neq i$ , so we must have  $[C_j] = 0 \in H_1(\mathbb{R}P^2; \mathbb{Z})$ . But  $L$  is nullhomologous, so

$[\cup_j C_j] = 0 \in H_1(\mathbb{RP}^2; \mathbb{Z})$ . On the other hand,  $[\cup_j C_j] = [C_i] + \sum_{j \neq i} [C_j] \neq 0$ , a contradiction. We conclude that every Seifert circle  $C_i$  bounds a unique disk  $B_i \subseteq \mathbb{RP}^2$ .

We now state the Seifert algorithm for links in  $\mathbb{RP}^3$ , which takes as an input a diagram  $D \subseteq \mathbb{RP}^2$  of a nullhomologous oriented link  $L \subseteq \mathbb{RP}^3$ , and outputs a Seifert surface  $F(D)$  in a canonical way (Step 3 has been modified to deal with Issue 2). See Figure 2.10 for an application of the algorithm.

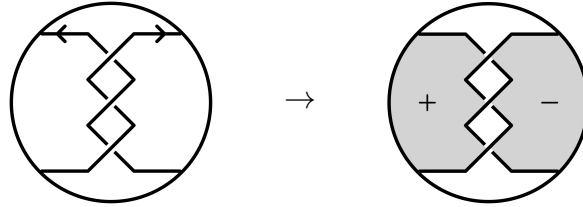


Figure 2.10: The Seifert algorithm applied to a diagram of a nullhomologous link.

**Algorithm 2.8** (Seifert algorithm in  $\mathbb{RP}^3$ ). *Step 1.* Perform oriented smoothings (see Figure 2.8) to obtain the Seifert circles  $C_i$ .

*Step 2.* Let  $B_i \subseteq \mathbb{RP}^2$  be the unique closed disk bounding  $C_i$ . Orient  $B_i$  such that  $C_i$  runs counterclockwise when the “up” side is viewed from above.

*Step 3.* Let  $d(C_i)$  denote the depth of  $C_i$  (defined as before). Let  $B_j$  be the maximal Seifert disk containing  $C_i$  in its interior. Translate  $B_i$  by  $d(C_i)$  units in the upwards direction assigned to  $B_j$  in Step 2.

*Step 4.* Attach half-twisted bands in accordance with the crossings of  $D$ .

With the Seifert algorithm at hand, we are now ready to prove Theorem 2.5.

*Proof of Theorem 2.5. Part 1: Every Seifert surface of  $L$  is  $S$ -equivalent to an algorithm surface.* We follow the same lines as Lemma 2.3, putting a Seifert surface  $F$  in general position with respect to the projection map  $p : \mathbb{RP}^2 \times \mathbb{R} \rightarrow \mathbb{RP}^2$  and attaching tubes to eliminate instances of Configuration 3 (see Figure 2.6). We must, however, be careful to ensure that these tube

attachments preserve the orientability of  $F$ . So, if necessary, perform an ambient isotopy of the type pictured in Figure 2.11 before resolving with a tube. Note, in particular, that the resulting surface is not only an algorithm surface, but also a checkerboard surface.

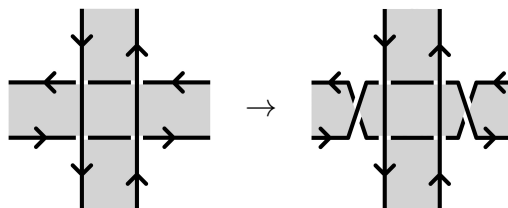


Figure 2.11: An ambient isotopy before attaching a thin tube.

*Part 2: Any two algorithm surfaces  $F$  and  $F'$  of  $L$  are  $S$ -equivalent.* Let  $D$  be the diagram determining  $F$  and  $D'$  the diagram determining  $F'$ . If  $D'$  is obtained from  $D$  by a single Reidemeister 1 move (see Figure 2.2), then clearly  $F'$  is ambient isotopic to  $F$  (see Move 2 of Figure 4, with  $F$  the white surface). A similar analysis reveals that the Reidemeister 2 and 3 moves also induce  $S$ -equivalences on the level of algorithm surfaces (see [2]), hence completing the proof.  $\square$

# Chapter 3

## The Parity of a Surface in $\mathbb{RP}^3$

§3.1 gives the basics of linking numbers in  $\mathbb{RP}^3$ , and §3.2 introduces *parity*, an invariant of surfaces which determines whether a given surface is  $S^*$ -equivalent to a Seifert surface.

### 3.1 Linking Number

**Definition 3.1.** Let  $K_1, K_2 \subseteq \mathbb{RP}^3$  be disjoint oriented knots and denote by  $q \in \{1, 2\}$  the quantity  $q = [K_1] + 1$  (here  $[K_1]$  denotes the image of  $K_1$  in  $H_1(\mathbb{RP}^3; \mathbb{Z}) = \{0, 1\}$ ). Let  $S \in C_2(\mathbb{RP}^3; \mathbb{Z})$  be a 2-cycle bounding  $qK_1$  and intersecting  $K_2$  in general position. We define the *linking number* of  $K_1$  and  $K_2$  to be the quantity

$$\text{lk}(K_1, K_2) = (S \cdot K_2)/q \in \left\{ \frac{n}{2} : n \in \mathbb{Z} \right\}.$$

Standard arguments show that this quantity is independent of our choice of  $S$ , is symmetric in  $K_1$  and  $K_2$ , and extends by linearity to a  $\frac{1}{2}\mathbb{Z}$ -valued function on pairs of disjoint oriented links [9, §2].

**Definition 3.2.** Let  $D \subseteq \mathbb{RP}^2$  be a diagram of an oriented link  $L \subseteq \mathbb{RP}^3$ . For a crossing  $c$  of  $D$ , define  $\text{writhe}(c) = +1$  if the orientation of  $L$  satisfies the right-hand rule at  $c$ , and define  $\text{writhe}(c) = -1$  otherwise.

We open with two remarks.

**Remark 3.3.** Let  $p : S^3 \rightarrow \mathbb{RP}^3$  be the 2-fold cover. Let  $L_1$  and  $L_2$  be disjoint oriented links in  $\mathbb{RP}^3$ . Then

$$\text{lk}(L_1, L_2) = \frac{1}{2} \text{lk}(p^{-1}L_1, p^{-1}L_2).$$

**Remark 3.4.** Let  $D \subseteq \mathbb{RP}^2$  be a disk diagram of an oriented link  $L \subseteq \mathbb{RP}^3$ . Note that the inverse image of  $D$  in  $S^2$  is a diagram of  $p^{-1}L$ . To each crossing of  $D$  is associated two crossings of  $p^{-1}D$ , each of the same writhe.

Combining Remarks 3.3 and 3.4 yields the following.

**Remark 3.5.** Returning to the situation where  $L_1, L_2 \subseteq \mathbb{RP}^3$  are disjoint oriented links, let  $D$  be a diagram of  $L_1 \cup L_2$ . Combining Remarks 3.3 and 3.4, we find that

$$\text{lk}(L_1, L_2) = \frac{1}{2} \sum \text{writhe}(c),$$

where the sum is taken over all crossings  $c$  of  $D$  involving both  $L_1$  and  $L_2$ .

We illustrate these remarks with an example.

**Example 3.6.** Figure 3.1 depicts a diagram in  $S^2$  of the preimage in  $S^3$  of a 2-component oriented link  $L = L_1 \cup L_2 \subseteq \mathbb{RP}^3$ . Each dotted circle  $C_i$  encloses a disk diagram  $D_i$  of  $L$ . We see that the singular crossing of  $D_i$  has exactly two preimages in  $S^2$ , each of the same writhe (+1). Let  $L'_i$  denote the preimage in  $S^3$  of  $L_i$ . The singular crossing of  $D_i$  has positive writhe, so the linking number  $\text{lk}(L_1, L_2)$  is computed as  $\text{lk}(L_1, L_2) = (\frac{1}{2})(+1) = \frac{1}{2}$ . Working instead in  $S^3$ , we see that  $\text{lk}(L'_1, L'_2) = 1$ , so  $\text{lk}(L_1, L_2) = \frac{1}{2}\text{lk}(L'_1, L'_2) = \frac{1}{2}$ .

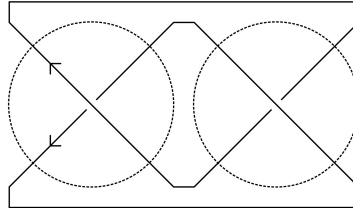


Figure 3.1: A diagram of the preimage in  $S^3$  of a link in  $\mathbb{RP}^3$ .

**Definition 3.7.** A link  $L \subseteq \mathbb{RP}^3$  is said to be *affine* if there exists an embedded open 3-ball  $B \subseteq \mathbb{RP}^3$  such that  $L \subseteq B$ .

Equivalently,  $L \subseteq \mathbb{RP}^3$  is affine if there exists an embedded projective plane  $\mathbb{RP}^2 \subseteq \mathbb{RP}^3$  such that  $L \cap \mathbb{RP}^2 = \emptyset$ . Note, in particular, that affine links are necessarily nullhomologous.

From the preceding discussion, it should be clear that for affine links, this notion of linking number agrees with the classical notion, and that  $\text{lk}(L_1, L_2) \in (\frac{1}{2}\mathbb{Z}) \setminus \mathbb{Z}$  if and only if  $L_1$  and  $L_2$  are both homologically nontrivial.

## 3.2 The Parity of a Surface in $\mathbb{RP}^3$

We motivate this subsection with the following problem. Consider the leftmost diagram of Figure 2.4, which depicts a knot  $K \subseteq \mathbb{RP}^3$  with checkerboard surfaces  $B$  and  $W$ . Theorems 2.2 and 2.5 imply that exactly one of the surfaces  $B$  or  $W$  is  $S^*$ -equivalent to an orientable surface. Yet clearly  $B$  and  $W$  are both nonorientable, so how do we deduce which is  $S^*$ -equivalent to an orientable surface?

To this end, we briefly discuss Euler and Betti numbers, from which a new invariant is defined: the *parity* of a surface.

### 3.2.1 Euler number

**Definition 3.8.** Let  $L \subseteq \mathbb{RP}^3$  be an oriented link with spanning surface  $F$ . Let  $L'$  denote a parallel copy of  $L$  disjoint from  $F$  (i.e.  $L'$  is the  $F$ -pushoff of  $L$ ). The *Euler number*  $e(F, L)$  is defined by  $e(F, L) = -\text{lk}(L, L')$ .

Since  $L$  and  $L'$  are nullhomologous, one immediately deduces that the Euler number of  $F$  is even. If  $F$  is a checkerboard surface, then to each crossing is associated a *type* and an *index* according to Figure 3.2 (where  $F$  is the shaded surface).

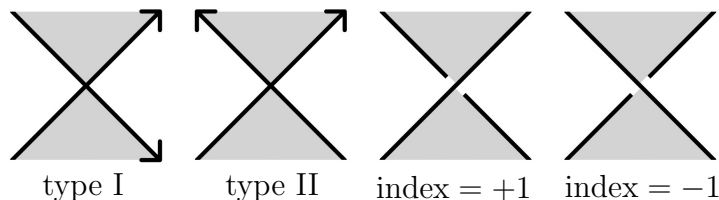


Figure 3.2: Type and index of a crossing.

Note that the type and index of a crossing depend on the checkerboard surface under consideration, and that if  $B$  and  $W$  are dual checkerboard surfaces, then  $\text{index}_B(c) = -\text{index}_W(c)$  at every crossing  $c$ .

By Remark 3.5, the Euler number is calculated as a weighted sum of crossings. In particular, the weight of a type I crossing equals 0 (see Figure 3.3), so

$$e(F, L) = -2 \sum \text{index}(c), \quad (2)$$

with the sum being taken over all type II crossings  $c$ .

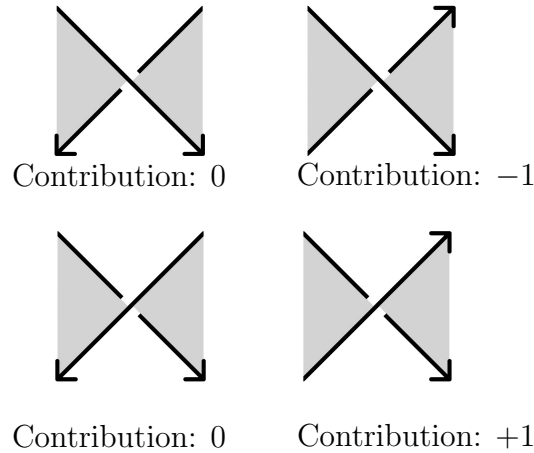


Figure 3.3: Local contributions to  $\frac{1}{2}e(F, L)$  at a crossing ( $F$  is the shaded surface).

### 3.2.2 Betti number

Recall that a checkerboard surface  $F$  can be conceived as a collection of disjoint regions lying in  $\mathbb{RP}^2$  (the so-called *faces* of  $F$ ) glued together via half-twisted bands (one for each crossing). A diagram  $D$  is said to be *cellularly embedded* if every component of  $\mathbb{RP}^2 \setminus D$  is an open disk. In particular, when  $D$  is cellularly embedded, the faces of  $B$  and  $W$  will all be disks.

**Lemma 3.9.** *Let  $B$  and  $W$  be the checkerboard surfaces of a diagram  $D \subseteq \mathbb{RP}^2$ . Say  $W$  has  $\alpha$  faces, all disks. Then  $b_1(B) = \alpha$ . An explicit basis of  $H_1(B; \mathbb{Z})$  is found by fixing  $\alpha - 1$  faces of  $W$  and letting  $\gamma_i \in H_1(B; \mathbb{Z})$  be a simple closed curve wrapping once around the  $i^{\text{th}}$  face, with the final generator being any simple closed curve  $\lambda \in H_1(B; \mathbb{Z})$  which does not vanish under  $H_1(B; \mathbb{Z}) \rightarrow H_1(\mathbb{RP}^3; \mathbb{Z})$  and whose image in  $\mathbb{RP}^2$  under the projection map does not self-intersect.*

**Example 3.10.** As an application of Lemma 3.9, let us consider the checkerboard surfaces  $B$  and  $W$  of the leftmost diagram of Figure 2.4. Appealing to Lemma 3.9, we see at a glance that  $b_1(B) = 2 = b_1(W)$

(bases are depicted in Figure 3.4 below).

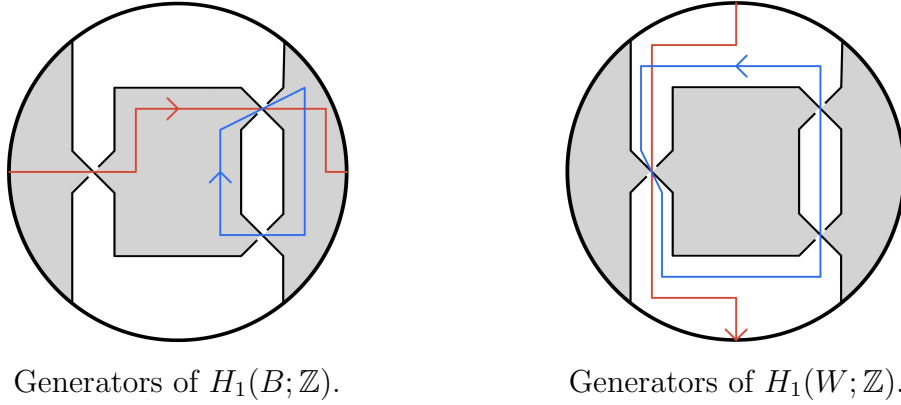


Figure 3.4: Homology of checkerboard surfaces.

To compute  $e(B, K)$  and  $e(W, K)$ , we start by orienting  $\partial B = K = \partial W$  so that the type II crossings may be identified (see Figure 3.5). Figure 3.3 then computes  $e(B, K) = -4$  and  $e(W, K) = +2$ .

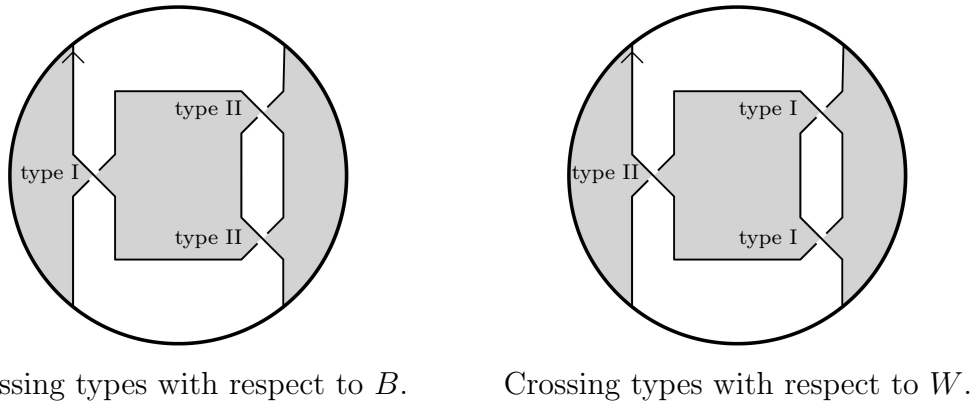


Figure 3.5: Crossing types.

*Proof of Lemma 3.9.* Up to homotopy equivalence,  $B$  can be conceived as a punctured  $\mathbb{RP}^2$  (one puncture for each face of  $W$ ). Starting with  $\mathbb{RP}^2$  and introducing a single puncture yields a mobius band, hence the generator  $\lambda$ . Every subsequent puncture introduces a new generator which simply wraps once around said puncture, hence the generators  $\gamma_i$ .  $\square$

**Definition 3.11.** A link  $L \subseteq \mathbb{RP}^3$  is called a *split link* if there exists an embedded closed 3-ball  $B \subseteq \mathbb{RP}^3$  whose interior and exterior both intersect  $L$ , but whose boundary is disjoint from  $L$ .

The takeaway of the preceding discussion on Betti numbers should be that when  $D$  is a cellularly embedded diagram of a nullhomologous link, the first Betti numbers  $b_1(B)$  and  $b_1(W)$  are easily computed, with explicit bases easily found. The following lemma shows that this covers all interesting cases.

**Lemma 3.12.** *Let  $D \subseteq \mathbb{RP}^2$  be a diagram of a non-split and non-affine link  $L \subseteq \mathbb{RP}^3$ . Then  $D$  is cellularly embedded.*

*Proof.* Assume  $D$  is not cellularly embedded. Then for some component  $Y$  of  $\mathbb{RP}^2 \setminus D$ , we have  $H_1(Y; \mathbb{Z}) \neq 0$ . Let  $\gamma \in H_1(Y; \mathbb{Z})$  be a homologically nontrivial simple closed curve. If  $\gamma$  vanishes under  $H_1(Y; \mathbb{Z}) \rightarrow H_1(\mathbb{RP}^3; \mathbb{Z})$ , then  $\gamma$  expresses  $L$  as a split link. Otherwise,  $\gamma$  expresses  $L$  as an affine link.  $\square$

### 3.2.3 Parity

**Definition 3.13.** Let  $L \subseteq \mathbb{RP}^3$  be an oriented link with spanning surface  $F$ . Define the *parity* of  $F$  to be the mod 2 quantity  $\text{Parity}(F, L) \in \{0, 1\}$  given by

$$\text{Parity}(F, L) = \left( b_1(F) + \frac{1}{2}e(F, L) \right) \bmod 2.$$

As seen in §3.2.1, the quantity  $e(F, L)$  is necessarily even, so parity is well-defined. Moreover, it is not hard to see that parity is invariant under  $S^*$ -equivalence of connected spanning surfaces. Indeed, it is clear that  $b_1(F)$  and  $e(F, L)$  are both invariant under ambient isotopies. As for attaching a thin tube, this move increases  $b_1(F)$  by 2 but does not affect  $e(F, L)$ . To complete the proof of  $S^*$ -invariance, note that attaching a small half-twisted band increases  $b_1(F)$  by 1, and changes  $\frac{1}{2}e(F, L)$  by  $\pm 1$ . We are now ready to address the motivating problem introduced at the start of this subsection.

**Theorem 3.14.** *Let  $L \subseteq \mathbb{RP}^3$  be a nullhomologous oriented link with connected spanning surface  $F$ . The following are equivalent.*

- (1)  $F$  is  $S^*$ -equivalent to a Seifert surface.
- (2)  $\text{Parity}(F, L) = 1 + |\{\text{components of } L\}| \bmod 2$ .

**Example 3.15.** We can now complete our investigation of the surfaces  $B$  and  $W$  of the leftmost diagram of Figure 2.4. In Example 3.10, we computed  $b_1(B) = 2 = b_1(W)$ ,  $e(B, K) = -4$ , and  $e(W, K) = +2$ . So,  $\text{Parity}(B, K) = 0$  and  $\text{Parity}(W, K) = 1$ . By Theorem 3.14, the surface  $B$  is  $S^*$ -equivalent to an orientable spanning surface (and  $W$  is not). Note that we only require knowledge of the parity of one of the surfaces  $B$  or  $W$  to determine which one is  $S^*$ -equivalent to an orientable spanning surface.

*Proof of Theorem 3.14.* (1)  $\Rightarrow$  (2) : Since parity is invariant under  $S^*$ -equivalence of connected spanning surfaces, there is no harm in assuming  $F$  is a connected Seifert surface. Then certainly  $b_1(F)$  equals  $1 + |\{\text{components of } L\}| \pmod{2}$ , and  $e(F, L) = 0$ , completing this direction of the proof.

(2)  $\Rightarrow$  (1) : Assume  $L$  is nonaffine. Since parity is invariant under  $S^*$ -equivalence of connected spanning surfaces and every spanning surface is  $S^*$ -equivalent to a checkerboard surface (Lemma 2.3), there is no harm in assuming  $F$  is a checkerboard surface. Then certainly there is some projective plane  $\mathbb{R}P^2 \subseteq \mathbb{R}P^3$  whose intersection with  $F$  is ribbon (see Figure 3.6–left). Let  $n$  denote the number of ribbon intersections (i.e. the number of components of  $F \cap \mathbb{R}P^2$ ). Recall that  $L$  is nonaffine, so  $n > 0$ . At each ribbon intersection, modify  $F$  as in Figure 3.6.



Figure 3.6: Resolving a ribbon intersection.

Denote by  $F \# \mathbb{R}P^2$  the spanning surface of  $L$  so obtained. If  $L$  is affine, let  $\mathbb{R}P^2 \subseteq \mathbb{R}P^3$  be an embedded projective plane missing  $L$ , and denote by  $F \# \mathbb{R}P^2$  the surface obtained by connecting  $F$  to  $\mathbb{R}P^2$  via a thin tube. In either case, an Euler characteristic computation reveals that  $b_1(F \# \mathbb{R}P^2) \equiv b_1(F) + 1 \pmod{2}$ , while certainly  $e(F \# \mathbb{R}P^2, L) = e(F, L)$ . So,  $\text{Parity}(F \# \mathbb{R}P^2, L) = \text{Parity}(F, L) + 1$ . Having already established the implication (1)  $\Rightarrow$  (2), it follows that  $F \# \mathbb{R}P^2$  is not  $S^*$ -equivalent to a Seifert surface. Since parity is invariant under  $S^*$ -equivalence of connected spanning surfaces, we also know that  $F \# \mathbb{R}P^2$  is not  $S^*$ -equivalent to  $F$ . By

Theorems 2.2 and 2.5, we conclude that  $F$  is  $S^*$ -equivalent to a Seifert surface, as desired.  $\square$

# Chapter 4

## The Gordon-Litherland Pairing

§4.1 introduces the *Gordon-Litherland pairing*, a symmetric bilinear map on the first homology group of a surface  $\mathcal{G}_F : H_1(F) \otimes H_1(F) \rightarrow \mathbb{Z}$ . This pairing leads to numerical invariants of nullhomologous oriented links in  $\mathbb{RP}^3$ . In §4.2 we discuss the elementary behaviour of these invariants, for example under reflections or connected sums. §4.3 describes an algorithm for computing the invariants, thereby revealing a plethora of new behaviours. Finally, the special case of alternating links is analyzed in §4.4. It is shown that alternating links admit definite spanning surfaces of opposite sign, and that special alternating links are chiral.

### 4.1 The Gordon-Litherland Pairing

**Definition 4.1.** Let  $F \subseteq \mathbb{RP}^3$  be a smoothly embedded compact surface without closed components. For a 1-cycle  $a \in C_1(F; \mathbb{Z})$ , let  $\tau a \in C_1(\mathbb{RP}^3 \setminus F; \mathbb{Z})$  denote the 1-cycle obtained by pushing  $a$  off of  $F$  in both normal directions. The symmetric bilinear map  $\mathcal{G}_F : H_1(F; \mathbb{Z}) \oplus H_1(F; \mathbb{Z}) \rightarrow \mathbb{Z}$  defined by  $\mathcal{G}_F(\alpha, \beta) = \text{lk}(\tau\alpha, \beta)$  is called the *Gordon-Litherland pairing* of  $F$ .

Note that  $\tau\alpha = 0 \in H_1(\mathbb{RP}^3; \mathbb{Z})$  for all  $\alpha \in H_1(F; \mathbb{Z})$ , so  $\mathcal{G}_F$  is integer-valued. To see that  $\mathcal{G}_F$  is well-defined, assume  $a, a' \in C_1(F; \mathbb{Z})$  are 1-cycles representing  $\alpha$ , and  $b, b' \in C_1(F; \mathbb{Z})$  are 1-cycles representing  $\beta$ . Let  $\overline{F} \rightarrow F$  be the orientation double cover. Conceiving of  $\tau$  as the transfer map  $H_1(F) \rightarrow H_1(\overline{F})$ , we see that  $a$  being homologous to  $a'$  implies  $\tau a$  is homologous to  $\tau a'$  as cocycles in  $\mathbb{RP}^3 \setminus F$ . It follows that  $\text{lk}(\tau a, b) =$

$\text{lk}(\tau a', b)$ . But  $b$  is homologous to  $b'$  within  $F$ , so  $\text{lk}(\tau a', b) = \text{lk}(\tau a', b')$ , proving that  $\mathcal{G}_F$  is well-defined. Symmetry will be demonstrated later on.

**Definition 4.2.** Let  $F$  a connected spanning surface of an oriented link  $L \subseteq \mathbb{R}P^3$ . The integer  $\sigma_F(L) = \text{sgn}(\mathcal{G}_F) + \frac{1}{2}e(F, L)$  is called the  $F$ -signature of  $L$  (here  $\text{sgn}(\mathcal{G}_F)$  denotes the signature of  $\mathcal{G}_F$ , calculated as the number of positive eigenvalues minus the number of negative eigenvalues). We also define the  $F$ -determinant and  $F$ -nullity by the formulas  $\det_F(L) = i^{b_1(F) + \frac{1}{2}e(F, L)} \det(\mathcal{G}_F)$  and  $\text{null}_F(L) = \text{null}(\mathcal{G}_F)$  (here  $i \in \mathbb{C}$  denotes the imaginary unit). It is often convenient to discuss all three quantities simultaneously. To this end, we define the *Gordon-Litherland numbers* of  $L$  determined by  $F$  to be the triple

$$\mathfrak{g}_F(L) = (\sigma_F(L), \det_F(L), \text{null}_F(L)).$$

**Proposition 4.3.** *The Gordon-Litherland numbers  $\mathfrak{g}_F(L)$  are invariant under  $S^*$ -equivalence of connected spanning surfaces.*

*Proof.* Suppose  $F$  and  $F'$  are connected spanning surfaces and  $F'$  is obtained from  $F$  by attaching a thin tube. The tube introduces two new generators to  $H_1(F'; \mathbb{Z})$  not present in  $H_1(F; \mathbb{Z})$ : a meridian  $m$  and a longitude  $l$ . So with respect to some basis  $a_1, \dots, a_m$  of  $H_1(F)$ , and an appropriately chosen basis  $a'_1, \dots, a'_m, m, l$  of  $H_1(F')$ , we have

$$\mathcal{G}_{F'} = \begin{bmatrix} \mathcal{G}_F & 0 & * \\ 0 & 0 & 1 \\ * & 1 & * \end{bmatrix}.$$

Let  $a''_i = a'_i - \mathcal{G}_F(a'_i, l)m$ . With respect to the basis  $a''_1, \dots, a''_m, m, l$ , we have

$$\mathcal{G}_{F'} = \begin{bmatrix} \mathcal{G}_F & 0 & 0 \\ 0 & 0 & 1 \\ 0 & 1 & * \end{bmatrix}. \quad (4.1)$$

In other words,  $\mathcal{G}_{F'}$  is a direct sum

$$\mathcal{G}_{F'} = \mathcal{G}_F \oplus \begin{bmatrix} 0 & 1 \\ 1 & * \end{bmatrix}.$$

It follows that  $\text{sgn}(\mathcal{G}_{F'}) = \text{sgn}(\mathcal{G}_F)$ ,  $\det(\mathcal{G}_{F'}) = -\det(\mathcal{G}_F)$ , and  $\text{null}(\mathcal{G}_{F'}) = \text{null}(\mathcal{G}_F)$ . Also,  $b_1(F') = b_1(F) + 2$  and  $e(F', L) = e(F, L)$ . Putting it all together, we see that  $\mathfrak{g}_F(L)$  is invariant under attaching thin tubes.

Now suppose  $F'$  is obtained from  $F$  by attaching a small half-twisted band. Then either  $\mathcal{G}_{F'} = \mathcal{G}_F \oplus [1]$ , in which case  $b_1(F') = b_1(F) + 1$  and  $e(F', L) = e(F, L) - 2$ ; or  $\mathcal{G}_{F'} = \mathcal{G}_F \oplus [-1]$ , in which case  $b_1(F') = b_1(F) + 1$  and  $e(F', L) = e(F, L) + 2$ . So,  $\mathfrak{g}_F(L)$  is invariant under attaching small half-twisted bands.  $\square$

**Definition 4.4.** Let  $F$  be a connected spanning surface of an oriented link  $L \subseteq \mathbb{RP}^3$ . If  $\text{Parity}(F, L) = 0$ , then define  $\mathfrak{g}_0(L) = \mathfrak{g}_F(L)$ . Otherwise, define  $\mathfrak{g}_1(L) = \mathfrak{g}_F(L)$ . In view of Theorems 2.5, 2.2, and 3.14, as well as Proposition 4.3, we see that to each nullhomologous oriented link  $L \subseteq \mathbb{RP}^3$  is associated two sets of invariants: the 0-signature, 0-determinant, and 0-nullity, given by the triple  $\mathfrak{g}_0(L)$ ; and the 1-signature, 1-determinant, and 1-nullity, given by the triple  $\mathfrak{g}_1(L)$ .

As an unordered pair, we have  $\{\mathfrak{g}_0(L), \mathfrak{g}_1(L)\} = \{\mathfrak{g}_B(L), \mathfrak{g}_W(L)\}$  for any dual checkerboard surfaces  $B$  and  $W$ . If we wish to compute the ordered pair  $(\mathfrak{g}_0(L), \mathfrak{g}_1(L))$ , we need only compute the parity of one of the surfaces  $B$  or  $W$  by the method described in §3.2.

Previous authors have considered the invariant  $|\det(\mathcal{G}_F)|$  (see, for example, [15] or [3]). Our sign-corrected determinant, which encodes the parity of  $F$ , is slightly stronger. For example, the checkerboard surfaces of the link depicted in the middle diagram of Figure 2.4 are distinguished by  $\det_F(L)$ , but not by  $|\det(\mathcal{G}_F)|$ .

## 4.2 Elementary Properties

Fix  $L \subseteq \mathbb{RP}^3$  a nullhomologous oriented link,  $n = |\{\text{components of } L\}| \pmod{2}$ , and  $F$  a connected spanning surface.

### 4.2.1 Reflection

Let  $L'$  and  $F'$  be obtained by reflection through a projective plane  $\mathbb{RP}^2 \subseteq \mathbb{RP}^3$ . Note that  $\mathcal{G}_{F'} = -\mathcal{G}_F$ ,  $b_1(F') = b_1(F)$ , and  $e(F', L') = -e(F, L)$ . It follows that

$$\mathfrak{g}_{F'}(L') = (-\sigma_F(L), i^{2b_1(F) - \frac{1}{2}e(F, L)} \det_F(L), \text{null}_F(L)).$$

Note, moreover, that the parities of  $F$  and  $F'$  coincide.

**Definition 4.5.** An oriented link  $L \subseteq \mathbb{RP}^3$  is said to be *achiral* if  $L$  is ambient isotopic to its reflection about an embedded projective plane  $\mathbb{RP}^2 \subseteq \mathbb{RP}^3$ . Otherwise,  $L$  is said to be *chiral*.

**Corollary 4.6.** *Let  $L \subseteq \mathbb{RP}^3$  be a nullhomologous oriented link. If  $\sigma_0(L) \neq 0$  or  $\sigma_1(L) \neq 0$ , then  $L$  is chiral.*

### 4.2.2 Split links

Let us now consider the case where our nullhomologous oriented link  $L \subseteq \mathbb{RP}^3$  is *split*. That is, there is some 3-ball  $\mathbb{D}^3 \subseteq \mathbb{RP}^3$  whose boundary is disjoint from  $L$ , but whose interior and exterior both intersect  $L$ . Let  $L_0 = L \cap \mathbb{D}^3$ , such that  $L = L_0 \sqcup L_1$ . Let  $F_0 \subseteq \text{int}(\mathbb{D}^3)$  be a connected spanning surface of  $L_0$ , and let  $F_1 \subseteq \mathbb{RP}^3 \setminus \mathbb{D}^3$  be a connected spanning surface of  $L_1$ . Any two spanning surfaces in  $\mathbb{R}^3$  of the same link are  $S^*$ -equivalent [23], so  $\text{Parity}(F_0, L_0) = 1 + |\{\text{components of } L_0\}|$ . Obtain a connected spanning surface  $F$  of  $L$  by connecting  $F_0$  and  $F_1$  via a thin tube. Then  $e(F, L) = e(F_0, L_0) + e(F_1, L_1)$  and  $\mathcal{G}_F$  decomposes as a direct sum  $\mathcal{G}_F = \mathcal{G}_{F_0} \oplus \mathcal{G}_{F_1} \oplus 0$ . So,

$$\mathfrak{g}_F(L_0 \sqcup L_1) = \left( \sigma_{F_0}(L_0) + \sigma_{F_1}(L_1), 0, \text{null}_{F_0}(L_0) + \text{null}_{F_1}(L_1) + 1 \right).$$

In view of Theorem 3.14, we see that  $\text{Parity}(F, L) = 1 + n$  if and only if  $\text{Parity}(F_1, L_1) = 1 + |\{\text{components of } L_1\}|$ .

**Corollary 4.7.** *If  $\det_0(L) \neq 0$  and  $\det_1(L) \neq 0$ , then  $L$  is not split.*

**Definition 4.8.** A link  $L \subseteq \mathbb{RP}^3$  is called a *boundary link* if  $L$  admits a disconnected spanning surface without closed components.

**Remark 4.9.** The same method used to prove Corollary 4.7 can also be used to prove that if an oriented link  $L$  is a boundary link, then  $\det_0(L) = 0$  or  $\det_1(L) = 0$ .

### 4.2.3 Connected sums

Take  $L_i$  and  $F_i$  as above, again noting that  $\text{Parity}(F_0, L_0) = 1 + |\{\text{components of } L_0\}|$ . Consider the *connected sum*  $L_0 \# L_1$ . This construction depends on a choice of diagram  $D$  expressing the link  $L_0 \sqcup L_1$  as a split link, and on a choice of two edges of  $D$  involved in the connected sum (one edge coming from  $L_0$ , the other from  $L_1$ ). The  $F_i$ 's determine a spanning

surface  $F$  of  $L_0 \# L_1$  in a natural way (see Figure 4.1).

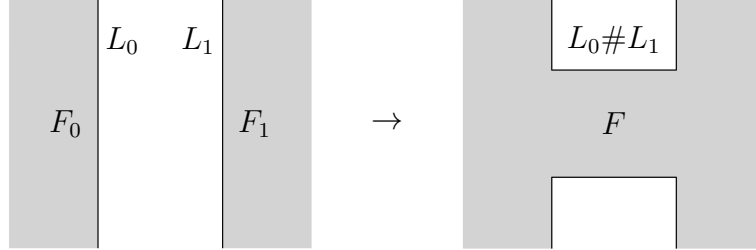


Figure 4.1: Connect sum link.

This time,  $e(F, L_0 \# L_1) = e(F_0, L_0) + e(F_1, L_1)$  and  $\mathcal{G}_F$  decomposes as  $\mathcal{G}_F = \mathcal{G}_{F_0} \oplus \mathcal{G}_{F_1}$ . So,  $\mathfrak{g}_F(L_0 \# L_1)$  equals

$$\left( \sigma_{F_0}(L_0) + \sigma_{F_1}(L_1), \det_{F_0}(L_0) \det_{F_1}(L_1), \text{null}_{F_0}(L_0) + \text{null}_{F_1}(L_1) \right).$$

Theorem 3.14 now dictates that  $\text{Parity}(F, L) = 1 + n$  if and only if the parity of  $F_1$  equals the number of components of  $L_1$  mod 2.

#### 4.2.4 Affine links

Suppose now that our oriented link  $L \subseteq \mathbb{R}P^3$  is affine. Let  $\mathbb{R}P^2 \subseteq \mathbb{R}P^3$  be a projective plane missing  $L$ , and let  $F \subseteq \mathbb{R}P^3 \setminus \mathbb{R}P^2$  be a spanning surface of  $L$ . Note that  $\mathbb{R}P^3 \setminus \mathbb{R}P^2 \cong \mathbb{R}^3$ , and that any two spanning surfaces in  $\mathbb{R}^3$  of the same link are  $S^*$ -equivalent [23]. So,  $\text{Parity}(F, L) = 1 + n$ . Let  $F'$  be the spanning surface obtained by connecting  $F$  to  $\mathbb{R}P^2$  via a thin tube. Then certainly  $\text{Parity}(F', L) = \text{Parity}(F, L) + 1$ , so that  $\text{Parity}(F', L) = n$ . Note, moreover, that  $\mathcal{G}_{F'} = \mathcal{G}_F \oplus 0$ , which implies

$$\mathfrak{g}_n(L) = \left( \sigma_{1+n}(L), 0, \text{null}_{1+n}(L) + 1 \right).$$

**Corollary 4.10.** *Let  $L \subseteq \mathbb{R}P^3$  be a nullhomologous oriented link. If any of the following conditions are satisfied, then  $L$  is nonaffine.*

- (1)  $\sigma_0(L) \neq \sigma_1(L)$
- (2)  $\det_n(L) \neq 0$
- (2)  $\text{null}_n(L) = 0$ .

### 4.3 Computing the Gordon-Litherland Pairing

Let  $D \subseteq \mathbb{RP}^2$  be a cellularly embedded diagram of a nullhomologous oriented link  $L \subseteq \mathbb{RP}^3$  (by Lemma 3.12, this covers all interesting cases). Let  $B$  and  $W$  be the checkerboard surfaces of  $D$ . Fix  $\alpha, \beta \in H_1(B; \mathbb{Z})$  cycles intersecting in general position and away from crossings. Note that local contributions to  $\mathcal{G}_B(\alpha, \beta)$  are made only when  $\alpha$  crosses over  $\beta$  or vice versa (i.e. only at crossings). In particular, when an arc of  $\alpha$  and an arc of  $\beta$  pass through a common crossing in the same direction, the local contribution to  $\mathcal{G}_B(\alpha, \beta)$  is precisely the  $B$ -index of the crossing (see Figure 3.2). Bilinearly extending this observation allows us to compute  $\mathcal{G}_B(\alpha, \beta)$  as the sum of local contributions at each crossing. Since the local contributions observed are symmetric in  $\alpha$  and  $\beta$ , we have the following.

**Corollary 4.11.** *The Gordon-Litherland pairing is symmetric.*

*Proof.* Let  $F$  be a connected spanning surface of  $L$ . Then  $F$  is  $S^*$ -equivalent to a checkerboard surface  $F'$  (see Lemma 2.3). By the local contributions to  $\mathcal{G}_{F'}$  observed above,  $\mathcal{G}_{F'}$  is symmetric. By the behaviour of  $\mathcal{G}_F$  under  $S^*$ -equivalence noted in §4.1, we see that  $\mathcal{G}_F$  is also symmetric.  $\square$

So, we have a definitive algorithm for computing the invariants  $\mathfrak{g}_0(L)$  and  $\mathfrak{g}_1(L)$  from a given diagram  $D$ . Start by checkerboard colouring  $D$  to obtain the dual checkerboard surfaces  $B$  and  $W$  (see §2.2). Next, compute the Betti numbers  $b_1(B)$  and  $b_1(W)$  by invoking Lemma 3.9, as well as the Euler numbers  $e(B, L)$  and  $e(W, L)$  (see §3.2.1). Use the bases provided by Lemma 3.9, as well as the computation of the Gordon-Litherland pairing as a weighted sum of crossings just discussed, to compute explicit matrices representing  $\mathcal{G}_B$  and  $\mathcal{G}_W$ . The data collected up to this point is enough to compute the unordered pair  $\{\mathfrak{g}_0(L), \mathfrak{g}_1(L)\}$ . Computing the ordered pair  $(\mathfrak{g}_0(L), \mathfrak{g}_1(L))$  is now just a matter of computing the parity of one of the surfaces  $B$  or  $W$ .

**Example 4.12.** Recall the bases of the checkerboard surfaces  $B$  and  $W$

obtained in Example 3.10 (see Figure 4.2).

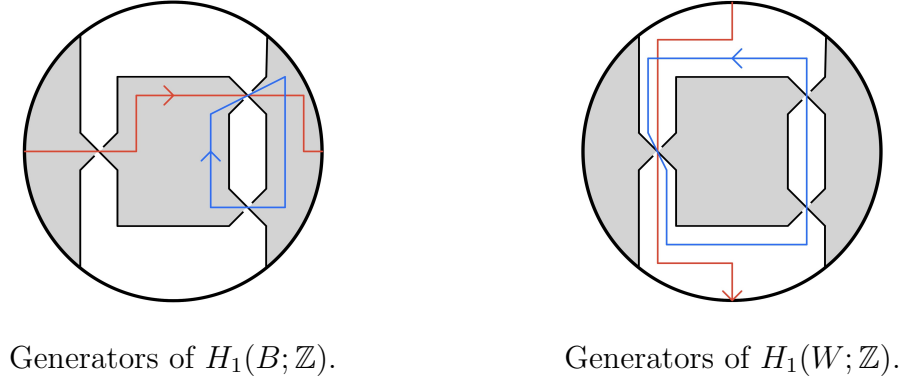


Figure 4.2: Dual checkerboard surfaces and their bases.

For the basis of  $H_1(B; \mathbb{Z})$ , let  $b_1$  be the curve in red, and let  $b_2$  be the curve in blue. Note that  $b_1$  and  $b_1$  have two crossings in common. Both crossings have  $B$ -index  $+1$  (see Figure 3.2 for the definition of index) and are crossed by  $b_1$  and  $b_1$  in the same direction. So,  $\mathcal{G}_B(b_1, b_1) = (+1) + (+1) = 2$ . Similarly,  $b_1$  and  $b_2$  have a single crossing in common. It has positive index and is passed through by both cycles in the same direction, so  $\mathcal{G}_B(b_1, b_2) = 1$ . By symmetry,  $\mathcal{G}_B(b_2, b_1) = 1$ . Finally, let us consider the self-linking  $\mathcal{G}_B(b_2, b_2)$ . The cycle  $b_2$  passes through two crossings. Both crossings have positive index, so  $\mathcal{G}_B(b_2, b_2) = 2$ . We conclude that with respect to the basis  $b_1, b_2$ , we have

$$\mathcal{G}_B = \begin{bmatrix} 2 & 1 \\ 1 & 2 \end{bmatrix}.$$

Similarly,

$$\mathcal{G}_W = \begin{bmatrix} -1 & -1 \\ -1 & -3 \end{bmatrix}.$$

In Example 3.10 we computed  $b_1(B) = 2 = b_1(W)$ ,  $e(B, K) = -4$ , and  $e(W, K) = +2$ . So  $\text{Parity}(B, K) = 0$  and we have all the information

needed to compute the Gordon-Litherland numbers  $\mathfrak{g}_0(K)$  and  $\mathfrak{g}_1(K)$ . Namely:

$$\begin{aligned}
\mathfrak{g}_0(K) &= \mathfrak{g}_B(K) \\
&= \begin{bmatrix} \sigma_B(K) \\ \det_B(K) \\ \text{null}_B(K) \end{bmatrix} \\
&= \begin{bmatrix} \text{sgn}(\mathcal{G}_B) + \frac{1}{2}e(B, K) \\ i^{b_1(B) + \frac{1}{2}e(B, K)} \det(\mathcal{G}_B) \\ \text{null}(\mathcal{G}_B) \end{bmatrix} \\
&= \begin{bmatrix} \text{sgn} \begin{bmatrix} 2 & 1 \\ 1 & 2 \end{bmatrix} + \frac{1}{2}(-4) \\ i^{2 + \frac{1}{2}(-4)} \det \begin{bmatrix} 2 & 1 \\ 1 & 2 \end{bmatrix} \\ \text{null} \begin{bmatrix} 2 & 1 \\ 1 & 2 \end{bmatrix} \end{bmatrix} \\
&= \begin{bmatrix} 0 \\ 3 \\ 0 \end{bmatrix}.
\end{aligned}$$

By a similar computation,  $\mathfrak{g}_1(K) = \mathfrak{g}_W(K) = (-1, -2i, 0)$ . In fact, it is no coincidence that  $\sigma_0(K)$  is even,  $\det_0(K)$  is odd, and  $|\det_1(K)|$  is even. In §4.3.1 we will see that these properties hold for any nullhomologous knot.

### 4.3.1 Consequences for knots

**Lemma 4.13.** *Let  $D \subseteq \mathbb{RP}^2$  be a diagram of a nullhomologous oriented link  $L \subseteq \mathbb{RP}^3$ . If  $D'$  is obtained from  $D$  by crossing changes, then we have mod 2 congruences  $|\det_0(L)| \equiv |\det_0(L')|$  and  $|\det_1(L)| \equiv |\det_1(L')|$ .*

*Proof.* Let  $B, W$  be checkerboard surfaces of  $D$ . Observe that  $B$  and  $W$  determine checkerboard surfaces  $B'$  and  $W'$  of  $D'$  in a natural way. Certainly,  $b_1(B) = b_1(B')$  (see Lemma 3.9) and the local contribution to  $e(B, L)$  at a crossing turns into its negative after a crossing change (see §3.2.1). So, the parities of  $B$  and  $B'$  coincide. Similarly, the local contribution to  $\mathcal{G}_B(\alpha, \beta)$  at a crossing turns into its negative after a crossing change. Thus, with respect to an appropriate choice of bases, we have an entry-wise mod 2 congruence  $\mathcal{G}_B \equiv \mathcal{G}_{B'}$ , so that  $\det(\mathcal{G}_B) \equiv \det(\mathcal{G}_{B'})$ . The same argument works with  $W$  and  $W'$ , so the proof is complete.  $\square$

**Theorem 4.14.** *Let  $K \subseteq \mathbb{RP}^3$  be a nullhomologous knot. Then  $|\det_0(K)|$  is odd and  $|\det_1(K)|$  is even.*

*Proof.* It is easily seen that for the affine unknot  $U \subseteq \mathbb{RP}^3$ , we have  $\det_0(U) = 1$  and  $\det_1(U) = 0$ . According to [17], there exists a sequence of crossing changes taking a diagram of  $K$  to a diagram of  $U$ . So, the result follows by Lemma 4.13.  $\square$

We observe two interesting corollaries of Theorem 4.14.

**Corollary 4.15.** *Let  $K \subseteq \mathbb{RP}^3$  be a nullhomologous knot. Then  $\sigma_0(K)$  is even.*

*Proof.* Let  $F$  be a connected and orientable spanning surface of  $K$ . Then  $b_1(F)$  is even and (by Theorem 4.14)  $\det(\mathcal{G}_F)$  is nonzero. It follows that  $\text{sgn}(\mathcal{G}_F)$  is even. But  $F$  is orientable, so

$$\sigma_0(K) = \sigma_F(K) = \text{sgn}(\mathcal{G}_F) + \frac{1}{2}e(F, K) = \text{sgn}(\mathcal{G}_F) + 0,$$

completing the proof.  $\square$

**Corollary 4.16.** *Let  $K_+ \subseteq \mathbb{RP}^3$  be a nullhomologous knot and let  $K_- \subseteq \mathbb{RP}^3$  be a knot obtained from  $K_+$  by turning a positive-writhe crossing  $c_+$  into a negative-writhe crossing  $c_-$ . Then*

$$\sigma_0(K_-) - \sigma_0(K_+) \in \{0, 2\}.$$

*Proof.* Let  $B_-$  (respectively,  $B_+$ ) be an algorithm surface of  $K_-$  (respectively,  $K_+$ ). Choose a basis of  $H_1(B_-; \mathbb{Z})$  such that the half-twisted band determined by  $c_-$  is crossed by exactly one basis element, exactly once. Call the basis element in question  $\alpha_-$ . Note that the matrices  $G_{B_-}$  and  $G_{B_+}$  will be identical in every entry save one. In particular,  $G_{B_-}(\alpha_-, \alpha_-) - G_{B_+}(\alpha_+, \alpha_+) = 2$ . Both  $G_{B_-}$  and  $G_{B_+}$  are non-degenerate by Theorem 4.14, so

$$\begin{aligned} \sigma_0(K_-) - \sigma_0(K_+) &= \text{sgn}(G_{B_-}) + \frac{1}{2}e(B_-, K_-) - (\text{sgn}(G_{B_+}) + \frac{1}{2}e(B_+, K_+)) \\ &= \text{sgn}(G_{B_-}) + 0 - (\text{sgn}(G_{B_+}) + 0) \\ &= \text{sgn}(G_{B_-}) - \text{sgn}(G_{B_+}) \\ &\leq 2. \end{aligned}$$

$\square$

**Definition 4.17.** For a nullhomologous oriented knot  $K \subseteq \mathbb{RP}^3$ , let  $u(K) \in \mathbb{Z}_{\geq 0}$  denote the minimum number of times  $K$  must pass through itself to obtain an affine unknot. By [17], the natural number  $u(K)$  exists.

As an immediate consequence of 4.16, we have the following.

**Proposition 4.18.** *If  $K \subseteq \mathbb{RP}^3$  is a nullhomologous knot, then*

$$|\sigma_0(K)| \leq 2u(K).$$

### 4.3.2 Consequences for links of two homologically non-trivial components

The methods of §4.3.1 can be adapted to obtain a plethora of similar results. For example, consider a nullhomologous oriented link  $L \subseteq \mathbb{RP}^3$  comprised of two homologically nontrivial components  $L = L_0 \cup L_1$ . Let  $U_2$  denote oriented link depicted in Figure 4.3.

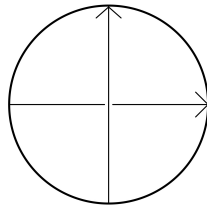


Figure 4.3: Diagram of  $U_2$ .

According to [17], a diagram of  $L$  can be turned into a diagram of  $U_2$  via crossing changes. Replicating the proof of Theorem 4.14, we obtain the following.

**Theorem 4.19.** *Let  $L \subseteq \mathbb{RP}^3$  be an oriented link comprised of two homologically non-trivial components. Then  $|\det_0(L)|$  and  $|\det_1(L)|$  are both odd numbers.*

Replicating the proofs of Corollaries 4.15 and 4.16 yields the following.

**Corollary 4.20.** *Let  $L \subseteq \mathbb{RP}^3$  be an oriented link comprised of two homologically nontrivial components. Then  $\sigma_1(L)$  is odd.*

**Corollary 4.21.** *Let  $L_+ \subseteq \mathbb{RP}^3$  be an oriented link comprised of two homologically nontrivial components. Let  $L_- \subseteq \mathbb{RP}^3$  be an oriented link obtained from  $L_+$  by turning a positive-writhe crossing into a negative writhe crossing. Then*

$$\sigma_1(L_-) - \sigma_1(L_+) \in \{0, 2\}.$$

**Definition 4.22.** For an oriented link  $L \subseteq \mathbb{RP}^3$  of two homologically non-trivial components, let  $u(L)$  denote the minimum number of times  $L$  must pass through itself to obtain the link  $U_2$  of Figure 4.3. The natural number  $u(L) \in \mathbb{Z}_{\geq 0}$  exists by [17].

**Proposition 4.23.**

$$|\sigma_1(L)| \leq 2u(L) + 1.$$

### 4.3.3 Unoriented links

The author has restricted the scope of the present paper to oriented links, but it is worth noting that much of the theory developed up to this point works just as well for unoriented links. For example, Theorem 2.2 has no dependence on the orientation of our link  $L$ . On the other hand, Theorem 2.5 depends vitally on the orientation of our link, as demonstrated by the middle diagram in Figure 2.4 (whose checkerboard surfaces are both orientable). One can, however, still distinguish the two  $S^*$ -equivalence classes using parity.

To define the parity of a surface without invoking an orientation on its boundary, we must first define an “unoriented Euler number.” Let  $F$  be a spanning surface of an unoriented link  $L \subseteq \mathbb{RP}^3$ . Write  $L = K_1 \cup \cdots \cup K_n$ . Endow each  $K_i$  with an orientation and let  $K'_i$  denote a parallel copy of  $K_i$  missing  $F$  (i.e.  $K'_i$  is the  $F$ -pushoff of  $K_i$ ). Let  $e(F) = -\sum_i \text{lk}(K_i, K'_i)$  (note that this does not depend on how we have oriented the  $K_i$ 's). One is then naturally inclined to define  $\text{Parity}(F) = b_1(F) + \frac{1}{2}e(F) \pmod{2}$ . As before, this quantity is easily computed when  $F$  is a checkerboard surface.

Now, although Seifert surfaces can no longer distinguish the two  $S^*$ -equivalence classes in the case of an unoriented link  $L$ , parity does the job just fine. Indeed, it is easily checked that  $\text{Parity}(F)$  is invariant under  $S^*$ -equivalence of connected spanning surfaces, and the proof of Theorem 3.14 translates seamlessly to prove that the two  $S^*$ -equivalence classes will have different parities.

As for the Gordon-Litherland numbers, one defines  $\sigma_F(L) = \text{sgn}(\mathcal{G}_F) + \frac{1}{2}e(F)$ ,  $\det_F(L) = i^{b_1(F) + \frac{1}{2}e(F)} \det(\mathcal{G}_F)$ , and  $\text{null}_F(L) = \text{null}(\mathcal{G}_F)$ . As before, we denote by  $\mathfrak{g}_F(L)$  the triple  $\mathfrak{g}_F(L) = (\sigma_F(L), \det_F(L), \text{null}_F(L))$  and we define  $\mathfrak{g}_i(L) = \mathfrak{g}_F(L)$  if  $F$  is a connected spanning surface with  $\text{Parity}(F) = i$  (here  $i = 0, 1$ ).

The computation of these unoriented invariants is just as easy as the oriented case. Much of the behaviour observed in §4.2 and §4.3 admits an unoriented analogue. We highlight, in particular, Corollaries 4.6, 4.7, and 4.10, as well as Lemma 4.13 and Theorems 4.14 and 4.19, which admit obvious unoriented analogues.

## 4.4 Alternating Links

Let  $L \subseteq \mathbb{RP}^3$  be a link with diagram  $D \subseteq \mathbb{RP}^2$ . Recall that a local orientation at a crossing  $c$  can be thought of as an isomorphism  $H_2(\mathbb{RP}^2, \mathbb{RP}^2 \setminus \{c\}) \rightarrow \mathbb{Z}$ . Let  $c$  and  $c'$  be crossings which cobound an edge  $e$  of  $D$ . Choose

a local orientation at  $c$  such that  $e$  is an overpass at  $c$ . This choice, together with the edge  $e$ , determines a local orientation at  $c'$ . We say that  $D$  satisfies the alternating condition at  $e$  if  $e$  is an underpass at  $c'$  with respect to this choice of local orientation.  $D$  is an *alternating diagram* if the alternating condition is satisfied at every edge.  $L$  is *alternating* if  $L$  admits an alternating diagram. The left and middle diagrams of Figure 2.1 depict alternating diagrams, while the right diagram depicts a non-alternating diagram.

As observed in [5], alternating links in  $\mathbb{RP}^3$  are necessarily nullhomologous. This can be seen by combining the alternating condition with the fact that a pair of simple closed curves in  $\mathbb{RP}^2$  will intersect in an odd number of points if and only if both curves are homologically nontrivial (a basic exercise in algebraic topology). In particular, alternating diagrams are checkerboard colourable. Let  $B$  and  $W$  be the checkerboard surfaces of a diagram  $D \subseteq \mathbb{RP}^2$ . Note that if  $L$  is non-split, then  $D$  is alternating if and only if  $\text{index}_B(c)$  is constant as  $c$  ranges over all crossings of  $D$  (see Figure 3.2 for the definition of the index at a crossing). In view of the local contributions to the Gordon-Litherland pairing observed in §4.3, the following theorem should therefore come as no surprise.

**Theorem 4.24.** *Let  $D \subseteq \mathbb{RP}^2$  be an alternating diagram of a non-split and non-affine link  $L \subseteq \mathbb{RP}^3$ . If  $B$  and  $W$  are the checkerboard surfaces of  $D$ , then  $B$  and  $W$  are definite and of opposite sign.*

That is,  $\mathcal{G}_B$  is positive-definite and  $\mathcal{G}_W$  is negative-definite, or vice-versa.

*Proof.* Without loss of generality, take every crossing to have  $B$ -index  $+1$  and  $W$ -index  $-1$ . By Lemma 3.12, the faces of  $B$  are all disks. So,  $B$  may be conceived as a collection of disjoint disks in  $\mathbb{RP}^2$  glued together via half-twisted bands (in particular, right-handed half-twists). An arc  $a$  passing through one of these half-twisted bands will have a local contribution of  $+1$  to  $\mathcal{G}_B(a, a)$ . Similarly, two arcs,  $a$  and  $b$ , passing in the same direction through a half-twisted band will have a local contribution of  $+1$  to  $\mathcal{G}_B(a, b)$ .

Let  $\gamma \in H_1(B; \mathbb{Z})$  be nonzero. We may express  $\gamma$  as a sum of simple closed curves  $\gamma = \gamma_1 + \cdots + \gamma_m$  such that for  $i \neq j$ , we have  $\gamma_i$  intersecting  $\gamma_j$  finitely many times, always in transverse double points and away from crossings. Moreover, each  $\gamma_i$  is nonzero as an element of  $H_1(B; \mathbb{Z})$ . Now allowing  $i = j$ , note that if an arc  $a$  of  $\gamma_i$  and an arc  $b$  of  $\gamma_j$  cross the same half-twisted band in opposite directions, then we can modify  $\gamma$  as in Figure 4.4 without affecting the image of  $\gamma$  in  $H_1(B; \mathbb{Z})$ . So, we may assume that any time  $\gamma_i$  and  $\gamma_j$  cross the same half-twisted band, they do so in the same direction. Since the local contributions to  $\mathcal{G}_B(\gamma_i, \gamma_j)$  occur only at

crossings, it follows that  $\mathcal{G}_B(\gamma_i, \gamma_j) \geq 0$ . Hence,

$$\mathcal{G}_B(\gamma, \gamma) = \sum_{i,j} \mathcal{G}_B(\gamma_i, \gamma_j) \geq \sum_i \mathcal{G}_B(\gamma_i, \gamma_i).$$

So, it suffices to argue that  $\mathcal{G}_B(\gamma_i, \gamma_i) > 0$  for some  $i$ . By our discussion of local contributions at the start of this proof, this is equivalent to arguing that  $\gamma_i$  passes through at least one half-twisted band. Assume for contradiction  $\gamma_i$  does not pass through any half-twisted bands. If  $\gamma_i$  vanishes under  $H_1(B; \mathbb{Z}) \rightarrow H_1(\mathbb{RP}^3; \mathbb{Z})$ , then  $\gamma_i$  expresses  $L$  as a split link. Otherwise,  $\gamma_i$  expresses  $L$  as an affine link. We conclude that  $\mathcal{G}_B(\gamma_i, \gamma_i) > 0$  for all  $i$ , and thus  $\mathcal{G}_B(\gamma, \gamma) > 0$ . In other words,  $B$  is positive-definite. An identical argument shows that  $W$  is negative-definite.  $\square$

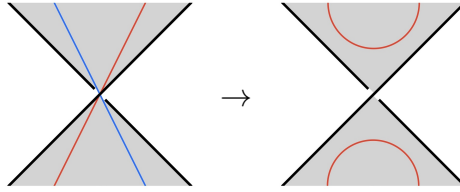


Figure 4.4: On the left,  $a$  is in red and  $b$  is in blue. The curve on the right has the same image in  $H_1(B; \mathbb{Z})$  as the curve on the left.

A *special alternating* link in  $\mathbb{RP}^3$  is an oriented link  $L \subseteq \mathbb{RP}^3$  admitting an alternating diagram  $D$  such that one of the checkerboard surfaces of  $D$  is a Seifert surface of  $L$ .

**Corollary 4.25.** *Let  $L \subseteq \mathbb{RP}^3$  be a special alternating link. If  $L$  is not the affine unknot, then  $L$  is chiral.*

*Proof.* Let  $F$  be the checkerboard Seifert surface of the alternating diagram  $D$ . Since  $L$  is not the affine unknot,  $b_1(F) \neq 0$ . By Theorem 4.24, we have  $\text{sgn}(\mathcal{G}_F) \neq 0$ . Since  $F$  is a Seifert surface,  $e(F, L) = 0$ . So,  $\sigma_F(L) = \text{sgn}(\mathcal{G}_F) \neq 0$ . By Corollary 4.6, we conclude that  $L$  is chiral, as desired.  $\square$

# Chapter 5

## Discussion

The *Greene-Howie Characterization Theorem* asserts that a non-split link in  $S^3$  is alternating if and only if it admits a pair of definite spanning surfaces of opposite sign [9][10]. In other words, it is a strong converse to (the  $S^3$  analogue of) Theorem 4.24. The Greene-Howie Theorem has also been established for links in thickened surfaces [4]. A vital ingredient in the proofs of Greene, Howie, and Boden and Karimi is a certain inequality involving a difference of signatures. In particular, if it were known that for nullhomologous oriented links  $L \subseteq \mathbb{RP}^3$ , we have  $|\sigma_0(L) - \sigma_1(L)| \leq 1$ , then the arguments of Greene and Howie should translate to the projective setting (modulo certain minor modifications). In fact, it would suffice to prove that  $|\sigma_F(L) - \sigma_{F'}(L)| \leq 1$  in the special case where  $F$  and  $F'$  are definite spanning surfaces of opposite sign. Unfortunately, the classical and thickened surface methods are quickly seen to be insufficient for establishing such an inequality in  $\mathbb{RP}^3$ .

It is natural to dream of an extension of the Characterization Theorem to all 3-manifolds admitting a nice diagrammatic theory of links (i.e. oriented thickenings of closed surfaces). It is therefore desirable to establish the Characterization Theorem in  $\mathbb{RP}^3$ , as the twisted  $I$ -bundle  $\mathbb{RP}^2 \tilde{\times} I$  is the simplest example of an oriented thickening of a closed nonorientable surface. The author hopes that this paper will lay the foundation for a proof of the Greene-Howie Characterization Theorem in  $\mathbb{RP}^3$ .

# Bibliography

- [1] Marta M Asaeda, Józef H Przytycki, and Adam S Sikora. Categorification of the Kauffman bracket skein module of I–bundles over surfaces. *Algebraic & Geometric Topology*, 4(2):1177–1210, 2004.
- [2] Dror Bar-Natan, Jason Fulman, and Louis H Kauffman. An elementary proof that all spanning surfaces of a link are tube-equivalent. *Journal of Knot Theory and its Ramifications*, 7:873–880, 1998.
- [3] Hans U. Boden, Micah Chrisman, and Homayun Karimi. The Gordon–Litherland pairing for links in thickened surfaces. *Internat. J. Math.*, 33(10-11):Paper No. 2250078, 47, 2022.
- [4] Hans U. Boden and Homayun Karimi. A characterization of alternating links in thickened surfaces. *Proceedings of the Royal Society of Edinburgh Section A: Mathematics*, 153(1):177–195, 2023.
- [5] Yulia V Drobotukhina. An analogue of the Jones polynomial for links in  $\mathbb{R}P^3$  and a generalization of the Kauffman–Murasugi theorem. *Algebra i analiz*, 2(3):171–191, 1990.
- [6] Yulia V Drobotukhina. Classification of links in  $\mathbb{R}P^3$  with at most 6 crossings. *Zapiski Nauchnykh Seminarov POMI*, 193:39–63, 1991.
- [7] Yulia V Drobotukhina. Classification of projective Montesinos links. *Algebra i Analiz*, 3(1):118–130, 1991.
- [8] Boštjan Gabrovšek. The categorification of the Kauffman bracket skein module of  $\mathbb{R}P^3$ . *Bulletin of the Australian Mathematical Society*, 88(3):407–422, 2013.
- [9] Joshua Greene. Alternating links and definite surfaces. *Duke Mathematical Journal*, 166(11):2133–2151, 2017.
- [10] Joshua Howie. A characterisation of alternating knot exteriors. *Geometry & Topology*, 21(4):2353–2371, 2017.

- [11] Vu Q Huynh and Thang TQ Le. Twisted Alexander polynomial of links in the projective space. *Journal of knot theory and its Ramifications*, 17(04):411–438, 2008.
- [12] Louis H Kauffman, Rama Mishra, and Visakh Narayanan. Knots in  $\mathbb{RP}^3$ . *arXiv preprint arXiv:2401.06050*, 2024.
- [13] Ciprian Manolescu and Michael Willis. A Rasmussen invariant for links in  $\mathbb{RP}^3$ . *arXiv preprint arXiv:2301.09764*, 2023.
- [14] Vassily O Manturov. Khovanov homology for virtual knots with arbitrary coefficients. *Izvestiya: Mathematics*, 71(5):967, 2007.
- [15] Cameron McA. Gordon and RA Litherland, On the signature of a link. *Invent. math*, 47(1):53–69, 1978.
- [16] Rama Mishra and Visakh Narayanan. Geometry of knots in real projective 3-space. *J. Knot Theory Ramifications*, 32(10):Paper No. 2350068, 24, 2023.
- [17] Maciej Mroczkowski. Diagrammatic unknotting of knots and links in the projective space. *Journal of Knot Theory and Its Ramifications*, 12(05):637–651, 2003.
- [18] Maciej Mroczkowski. Polynomial invariants of links in the projective space. *Fund. Math.*, 184:223–267, 2004.
- [19] Kunio Murasugi. On a certain numerical invariant of link types. *Transactions of the American Mathematical Society*, 117:387–422, 1965.
- [20] Jessica S Purcell and Lecheng Su. Alternating links on nonorientable surfaces and Klein-bottly alternating links. *arXiv preprint arXiv:2412.07133*, 2024.
- [21] Julia Viro and Oleg Viro. Fundamental groups in projective knot theory. In *Topology and geometry—a collection of essays dedicated to Vladimir G. Turaev*, volume 33 of *IRMA Lect. Math. Theor. Phys.*, pages 75–92. Eur. Math. Soc., Zürich, [2021] ©2021.
- [22] Oleg Yanovich Viro. Topological problems on lines and points of three-dimensional space. In *Doklady Akademii Nauk*, volume 284, pages 1049–1052. Russian Academy of Sciences, 1985.
- [23] Akira Yasuhara. An elementary proof for that all unoriented spanning surfaces of a link are related by attaching/deleting tubes and Möbius bands. *J. Knot Theory Ramifications*, 23(1):1450004, 5, 2014.